12 Advanced Anisotropy Concepts

In the preceding two chapters we described steady-state and time-resolved anisotropy measurements, and presented a number of biochemical examples that illustrate the types of information available from these measurements. Throughout these chapters we stated that anisotropy decay depends on the size and shape of the rotating species. However, the theory that relates the form of anisotropy decay to the shape of the molecule is complex, and was not described in detail. In the present chapter we provide an overview of the rotational properties of non-spherical molecules, as well as representative examples.

For the initial topic in this chapter we describe associated anisotropy decays. Such decays occur when the solution contains more than one type of fluorophore, or the same fluorophore in different environments. Such systems can result in complex anisotropy decays, even if the individual species each display a single-exponential anisotropy decay.

12.1. ASSOCIATED ANISOTROPY DECAY

Biochemical samples frequently contain multiple fluorophores or a single fluorophore in more than one environment. Such a sample can be expected to display a multi-exponential anisotropy decay. For a mixture the origin of the multiple decay times is different from the preceding two chapters. In these chapters we described how a single fluorophore bound to a biomolecule could display multiple correlation times as the result of segmental motions in addition to rotational diffusion. Multiple correlation times can also occur for non-spherical molecules (Section 12.3) or for long flexible molecules like DNA. In these cases the multiple correlation times are due to a single fluorophore displaying complex motion.

There is another possible origin of complex anisotropy decays, which is a mixture of fluorophores or a single fluorophore in two different environments. This concept is illustrated in Figure 12.1, which shows tryptophan in two environments: free in solution and as the single-tryptophan residue in human serum albumin (HSA). Tryptophan has a lifetime near 3 ns, and a correlation time in water near 50 ps. The single-tryptophan residue in HSA has a longer lifetime near 8 ns and a correlation time near 40 ns. We have assumed that the intensity and anisotropy decay are all single exponentials.

A mixture of fluorophores with correlation times of 40 ns and 50 ps can result in an unusual anisotropy decay. In Section 11.5 we described how rapid segmental motions result in an initial rapid decrease in the anisotropy decay of a protein, followed by a slower anisotropy decay at longer times due to overall rotational diffusion. The resulting anisotropy decay can be quite different if the same two correlation times are present in the sample, but are due to a mixture of fluorophores rather than a single fluorophore. Such a mixture can display a different type of anisotropy decay in which the anisotropy decreases to a minimum and then increases at longer times (Figure 12.2).

The origin of the unusual behavior seen in Figure 12.2 can be understood by examining the intensity and anisotropy decays of the individual species (Figure 12.3). At any time following excitation the anisotropy is given by the additivity law:

$$r(t) = f_1(t)r_1(t) + f_2(t)r_2(t) \qquad (12.1)$$

where $f_1(t)$ is the fractional intensity of the tryptophan and $f_2(t)$ is the fractional intensity of the HSA. The fractional intensity of each species can be calculated from the intensity decays. Assume that at $t = 0$ both species contribute equally. Because of its shorter 3-ns lifetime the fractional intensity of the tryptophan decreases more rapidly with time than the emission from HSA with a lifetime of 8 ns. The fractional contribution of tryptophan becomes smaller at longer times. However, at intermediate times, the low

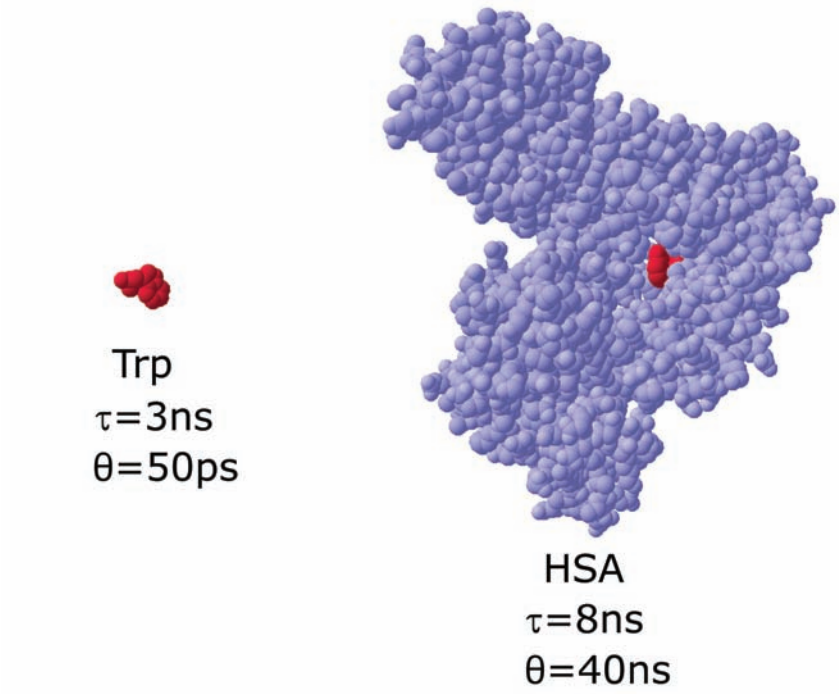

Figure 12.1. Model system for an associated anisotropy decay: a mixture of tryptophan in solution and in HSA.

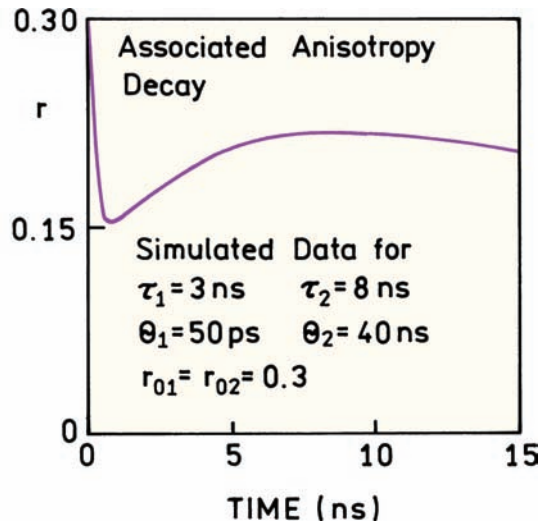

Figure 12.2. Simulated associated anisotropy decay simulated for a mixture of fluorophores, $\tau_1 = 3$ ns, $\theta_1 = 50$ ps, $\tau_2 = 8$ ns, $\theta_2 = 40$ ns, $r_{01} = r_{02} = 0.30$. The individual intensity and anisotropy decays are shown in Figure 12.3.

anisotropy of the tryptophan results in a transient decrease in the measured value of $r(t)$. At longer times, the emission becomes dominated by HSA with its larger anisotropy, resulting in an increase in $r(t)$.

12.1.1. Theory for Associated Anisotropy Decay

It is useful to compare the equations describing associated and non-associated anisotropy decays. For a single fluorophore that displays a multi-exponential intensity and anisotropy decay the parallel and perpendicular components of the emission are given by

$$I_{\parallel}(t) = \frac{1}{3} I(t)\left[1 + 2r(t)\right] \tag{12.2}$$

$$I_{\perp}(t) = \frac{1}{3} I(t)\left[1 - r(t)\right] \tag{12.3}$$

These expressions can be written in terms of the multiple exponential components in $I(t)$ and $r(t)$:

$$I_{\parallel}(t) = \frac{1}{3}\sum_i \alpha_i \exp(-t/\tau_i)\left[1 + 2\sum_j r_{0j} \exp(-t/\theta_j)\right] \tag{12.4}$$

$$I_{\perp}(t) = \frac{1}{3}\sum_i \alpha_i \exp(-t/\tau_i)\left[1 - \sum_j r_{0j} \exp(-t/\theta_j)\right] \tag{12.5}$$

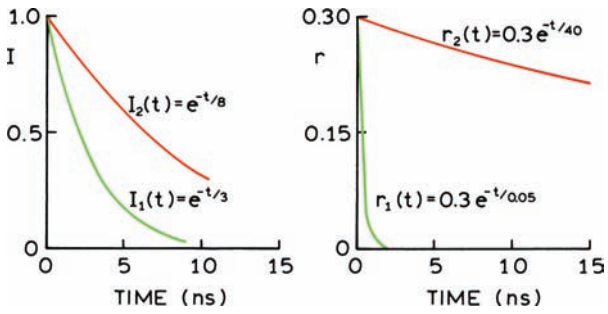

Figure 12.3. Intensity and anisotropy decays corresponding to the individual species shown in Figure 12.1.

For the non-associated decay there is a single intensity decay $I(t)$ and a single anisotropy decay, even though both decays can be multi-exponential. A non-associated decay describes the motions of a single type of fluorophore in a single environment.

For an associated system each fluorophore population displays its own intensity and anisotropy decay. The polarized intensity decays are given by

$$I_{\parallel}(t) = \frac{1}{3}\sum_m I_m(t)\left[1 + 2r_m(t)\right] \qquad (12.6)$$

$$I_{\perp}(t) = \frac{1}{3}\sum_m I_m(t)\left[1 - r_m(t)\right] \qquad (12.7)$$

where the subscript m represents each fluorophore population, and not a component of a multi-exponential decay. Each fluorophore population is described by a different intensity decay $I_m(t)$ and a different anisotropy decay $r_m(t)$.

The nature of an associated anisotropy decay can be understood by considering eqs. 12.6 and 12.7 for a two-component mixture. Assume each species displays a single lifetime (τ_m) and a single correlation time (θ_m). The amplitudes at $t = 0$ can be represented by α_m, which is the amplitude of the mth population at $t = 0$. The anisotropy decay for this mixture is then given by

$$r(t) = \frac{\sum_m \alpha_m \exp(-t/\tau_m)\, r_{0m} \exp(-t/\theta_m)}{\sum_m \alpha_m \exp(-t/\tau_m)} \qquad (12.8)$$

The fractional intensity of the mth component at any time t is given by

$$f_m(t) = \frac{\alpha_m \exp(-t/\tau_m)}{\sum_m \alpha_m \exp(-t/\tau_m)} \qquad (12.9)$$

and the time-dependent anisotropy is given by

$$r(t) = \sum_m f_m(t)\, r_m(t) \qquad (12.10)$$

This equation states that the anisotropy at time t is given by the intensity-weighted average of the anisotropies of each species at the same time. Equation 12.10 is the additivity law for anisotropies at each time in the total decay. More detailed descriptions of the theory for associated anisotropy decays can be found elsewhere.[1–8]

12.1.2. Time-Domain Measurements of Associated Anisotropy Decays

Experimental studies of associated anisotropy decays started with early reports on cis- and trans-parinaric acid.[9–11] The anisotropy was observed to increase at long times (Figure 12.4). In this case the probe cis-parinaric acid was covalently linked to the second position on a phosphatidylcholine molecule (cis-parinaroyl-PC).[12–13] The increase in anisotropy at times longer than 10 ns was explained as the result of a population of fluorophores with a longer life-

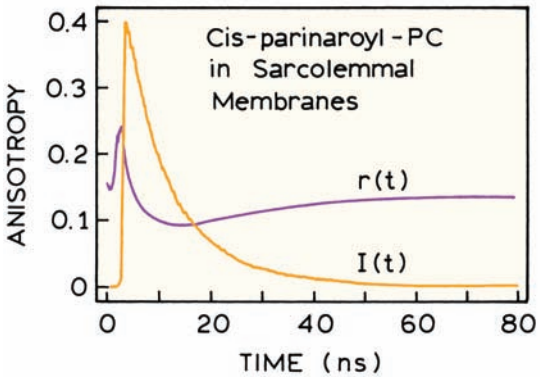

Figure 12.4. Intensity and anisotropy decay of cis-parinaroyl-PC in rat skeletal sarcolemmal membranes. From [12].

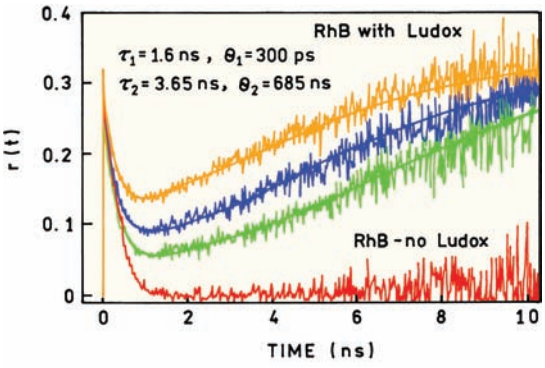

Figure 12.5. Anisotropy decay of rhodamine B in water and with 0.04, 0.08, and 0.27% Ludox (from bottom to top). For the highest silica concentration α_1 (H_2O) = 0.70 and α_2 (silica) = 0.30 (eq. 12.8). Revised from [18].

time, which also displayed restricted motion. Associated anisotropy decays have also been observed for labeled oligonucleotides when bound to proteins[14–15] and for rhodamine and proteins in lipid–protein systems.[16–17]

A dramatic example of an associated anisotropy decay is shown in Figure 12.5. These anisotropy decays were observed for rhodamine B (RhB) in the presence of Ludox, which is colloidal silica. In the absence of silica the RhB anisotropy decays rapidly to zero. In the presence of increasing amounts of silica (bottom to top) the anisotropy initially decreases and then increases to nearly the time-zero value.[18] The initial rate of anisotropy decay is similar to that observed without silica. This suggests that in all samples, with and without silica, the anisotropy for times less than 1 ns is due to RhB that is not bound to silica. It seems logical to conclude that the anisotropy at long times is due to RhB bound to the silica particles. Since the long-time anisotropy is close to the time-zero anisotropy, the correlation time of RhB bound to silica must be long.

Associated anisotropy decays cannot always be distinguished from non-associated decays.[1–3] For instance, if the lifetimes of RhB were the same when in water and when bound to silica, the observed anisotropy decay would be a multi-exponential but the anisotropy would not increase at

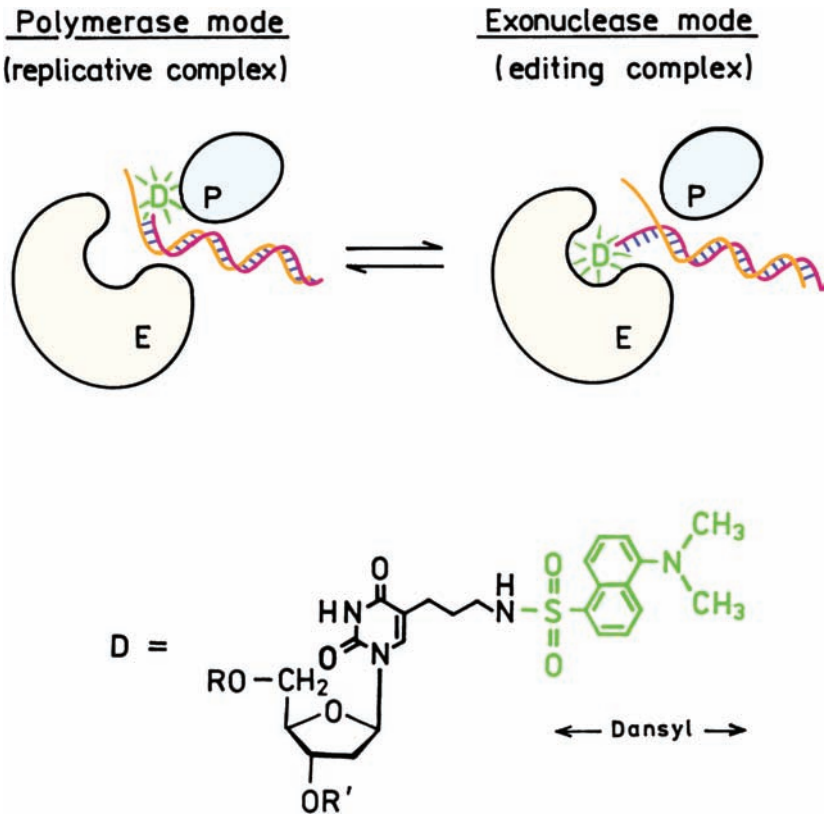

Figure 12.6. Klenow fragment of *E. coli* DNA polymerase with a bound DNA oligomer. The dansyl-labeled base (D) is located at the 10th residue from the 5' end of the 17-mer. Revised from [19].

long times (Problem 12.1). An increased anisotropy at long times requires that the species with a longer correlation time has a longer lifetime than the species with a short correlation time.

12.2. BIOCHEMICAL EXAMPLES OF ASSOCIATED ANISOTROPY DECAYS

12.2.1. Time-Domain Studies of DNA Binding to the Klenow Fragment of DNA Polymerase

DNA polymerase must replicate DNA with high accuracy. This requires that the polymerase be able to incorporate DNA bases into the nascent DNA primer strand and to remove incorrectly incorporated bases. The Klenow fragment (KF) from *E. coli* DNA polymerase is a single 68-kDa peptide that contains both the polymerase activity and the exonuclease activity (Figure 12.6). These activities are located at two different sites on the KF: the polymerase site and the exonuclease site. If a properly matched oligomer binds to the KF the shorter nascent chain is expected to bind to the polymerase site (left). If the DNA oligomer contains mismatched base pairs the nascent chain is expected to bind to the exonuclease site (right).

The mode of DNA binding to the KF was studied using dansyl-labeled DNA oligomers. These strands consisted of a 17-mer that contained the dansyl-labeled (D) base and a 27-mer that served as 7th template. These oligomers were either perfectly matched or contained 1 to 4 mismatched base pairs. Anisotropy decays of these oligomers bound to the KF are shown in Figure 12.7. When the oligomer is perfectly matched ($x = 0$) there is an associated anisotropy decay, as seen by the increasing anisotropy for times greater than 5 ns. As the number of mismatches increases from 1 to 4 the anisotropy decay loses the rising component and shows only the usual time-dependent decreases in anisotropy.

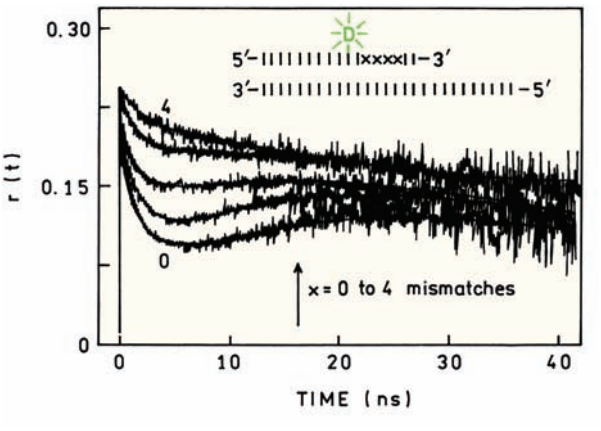

Figure 12.7. Anisotropy decay of the dansyl-labeled DNA oligomers when bound to the Klenow fragment. Revised from [19].

These anisotropy decays provide information about binding of the nascent strand for matched and mismatched oligomers. For the mismatched oligomers the non-associated anisotropy decay indicates the fluorophore is in a single type of environment. Since the anisotropy decay is slow the probe must be rigidly bound to the protein. Hence for mismatched oligomers, the 3' end of the nascent strand is firmly bound to the exonuclease site. For the matched oligomers some of the dansyl groups are freely rotating, resulting in a fast component in the anisotropy decay. The relative proportions of the 3' nascent strand end binding to each of the sites depends on the number of mismatched base pairs in the oligomer. The fractions of the dansyl probe bound to each site can be determined from the shape of the anisotropy decay.

The success of this experiment depended on the use of a dansyl-labeled oligomer, rather than fluorescein, rhodamine, or similar fluorophores. The lifetime of the dansyl group is sensitive to the surrounding polarity and/or rigidity. When the dansyl group was bound to the polymerase site it not only rotated more freely but also displayed a shorter lifetime than when bound rigidly to the exonuclease site. This shorter lifetime associated with the shorter correlation time is needed for unambiguous use of the associated model.

12.2.2. Frequency-Domain Measurements of Associated Anisotropy Decays

Associated anisotropy decays also result in unusual frequency-domain data.[20–21] This is shown by studies of ANS that is partially bound to apomyoglobin. Each apomyoglobin molecules binds only one ANS molecule, and the extent of binding is limited by using low concentrations of apomyoglobin. Frequency-domain anisotropy data for the system show differential phase angles which initially increase with frequency, and then decrease at higher frequencies (Figure 12.8). Surprisingly, the differential phase angles become negative even though the time-zero anisotropy is positive. This behavior is distinct from that observed for ANS when free in solution (○) or when completely bound to apomyoglobin (●, Figure 12.9). Data of the type shown in Figure 12.8 can be analyzed to recover

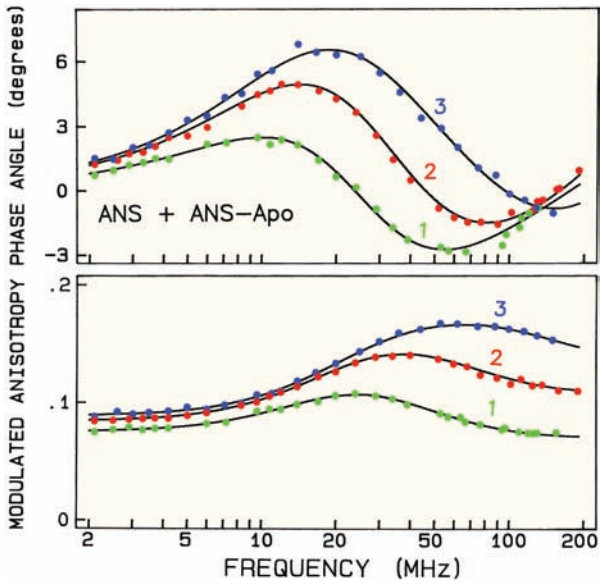

Figure 12.8. Frequency-domain anisotropy data for samples containing apomyoglobin ANS in molar ratios of 0.0087 (1), 0.0158 (2), and 0.079 (3). Reprinted from [20]. Copyright © 1987, with permission from Elsevier Science.

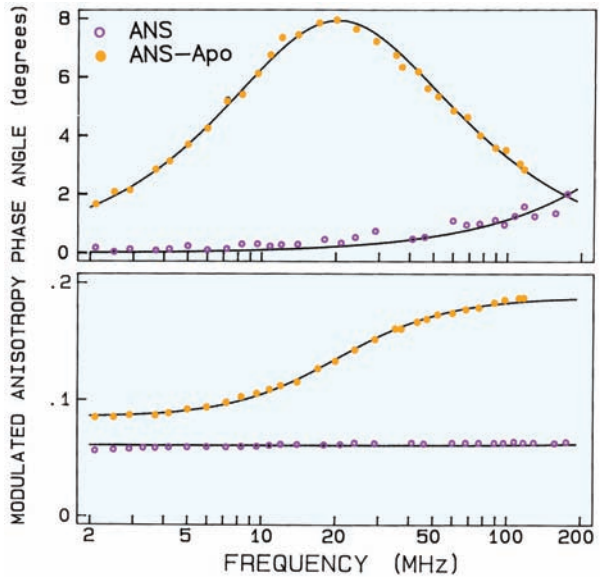

Figure 12.9. Frequency-domain anisotropy decays of apomyoglobin-ANS (●) and ANS alone (○). The correlation times are 13.2 ns for apomyoglobin–ANS and 97 ps for ANS alone. Reprinted from [20]. Copyright © 1987, with permission from Elsevier Science.

the time-zero anisotropies and correlation times of each fluorophore population.

To summarize, an anisotropy decay can be multi-exponential because a single population of fluorophores exhibits complex motions, as due to more than one population of fluorophores with different rotational behavior. Associated anisotropy decays can sometimes be identified from unusual anisotropy decays. However, depending upon the lifetimes and correlation times it may or may not be possible to identify the decay as associated or non-associated.

12.3. ROTATIONAL DIFFUSION OF NON-SPHERICAL MOLECULES: AN OVERVIEW

Time-resolved anisotropy measurements can be used to determine the size and shape of the rotating fluorophore. A fluorophore that rotates at different rates around different axes is said to display anisotropic rotational diffusion. The theory for anisotropic rotational diffusion is rather complex. Prior to describing the complex equations for this topic it is valuable to have an overview of the results. A rotating fluorophore macromolecule need not be symmetric about any axis. A totally unsymmetric shape can only be described by the shape itself, and is thus not useful for a general theory. Hence non-spherical molecules are described as being a general ellipsoid or an ellipsoid of revolution (Figure 12.10). An ellipsoid is a shape whose plane sections are all ellipses or circles. A general ellipsoid has three unequal semi-axes, $a \neq b \neq c$, and an ellipsoid of revolution has two equal axes and one unique axis. The rotational properties of ellipsoids are described in terms of the rotational rates or rotational diffusion coefficients (D) around each axis (D_1, D_2 and D_3). The theory for rotational diffusion of non-spherical molecules predicts the anisotropy decays for ellipsoids and ellipsoids of revolution. A non-spherical molecule can display three or more rotational correlation times.

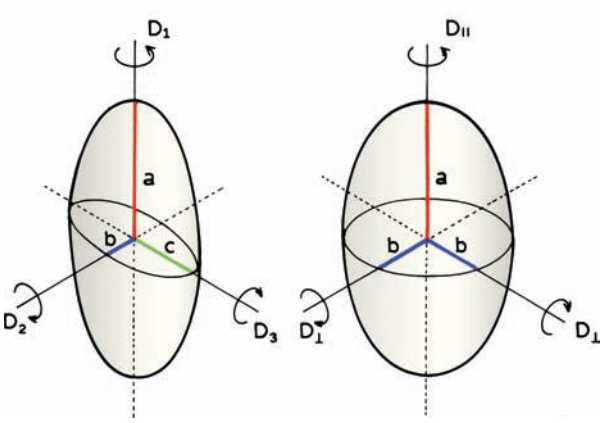

Figure 12.10. General ellipsoid with three unequal semi-areas $a \neq b \neq c$, and an ellipsoid of revolution ($a \neq b = c$).

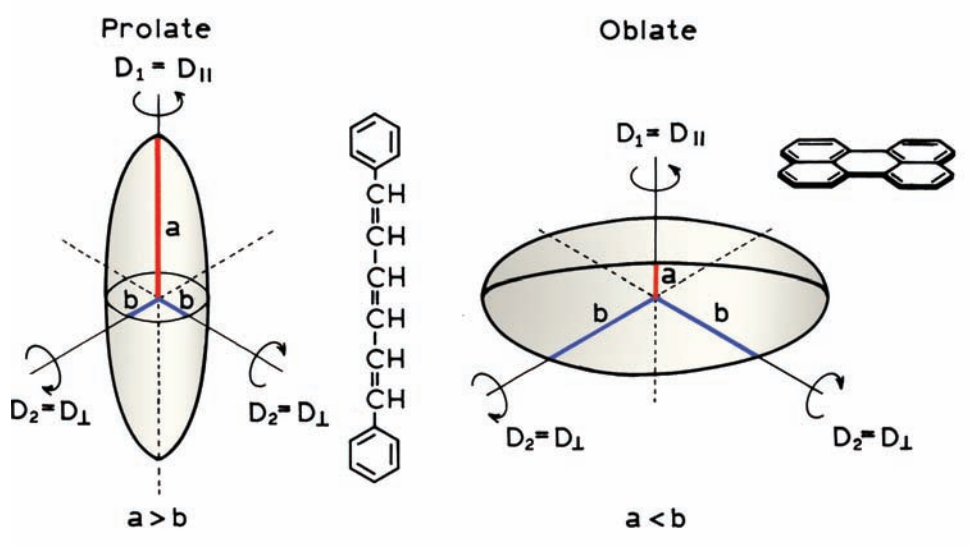

Figure 12.11. Prolate and oblate ellipsoids of revolution.

These correlation times are not simply equal to $1/6D$ for each of the rotational diffusion coefficients. Instead, the rotational correlation times in the anisotropy decay are functions of the rotational diffusion coefficients. That is, each of the rotational diffusion coefficients can contribute to each of the correlation times.

Most experiments cannot reveal the shape of a general ellipsoid, so that most data are interpreted in terms of the ellipsoids of revolution. Two cases are possible: the prolate and oblate ellipsoids of revolution. These shapes are often referred to as prolate or oblate ellipsoids. In a prolate ellipsoid the unique axis is longer than the other two equal axes ($a > b = c$). Prolate ellipsoids are elongated along the symmetry axis. A typical prolate ellipsoid would be DPH (Figure 12.11). For an oblate ellipsoid the unique axis is smaller than the other two equivalent axes ($a < b = c$). Oblate ellipsoids are shaped like flattened spheres. Perylene is an oblate ellipsoid.

Because of the two equivalent axes in ellipsoids of revolution, their hydrodynamics can be described with only two diffusion coefficients (Figure 12.11), but recall that the anisotropy decay measurements reveal correlation times and not the individual rotational diffusion coefficients. Rotation about the unique axis in either a prolate or oblate ellipsoid is called $D_{\|}$, and rotation about either of the other two equivalent axes is referred to as $D_{\perp}$. In general one can expect $D_{\|} > D_{\perp}$ for both prolate and oblate ellipsoids because rotation about the unique axis can occur with less displacement of solvent than rotation about the other two axes. However, small molecules do not always rotate as hydrodynamic objects, and prolate or oblate-shaped fluorophores may display more than two correlation times.

12.3.1. Anisotropy Decays of Ellipsoids

The theory for rotational diffusion of ellipsoids as measured by fluorescence polarization can be traced to the classic reports by F. Perrin.[22–25] Since these reports, the theory has been modified to include a description of expected anisotropy decays for molecules free in solution and in constrained environments.[26–37] For a rigid ellipsoid with three unequal axes the anisotropy decays with five correlation times.[28–30] The correlation times depend on the three rotation diffusion coefficients, and the amplitudes depend on the orientation of the absorption and emission transition moments within the fluorophore and/or ellipsoid. The theory predicts five correlation times, but it is known that two pairs of correlation times are very close in magnitude. In practice only three correlation times are expected for a non-spherical molecule.[31]

The anisotropy decays of non-spherical molecules depend on the orientation of the transition moments relative to the principle axes. The absorption and emission moments can have any arbitrary direction relative to the major (a) and minor (b) axes of the ellipsoid (Figure 12.12). The transition moments are not necessarily aligned with an axis of the ellipsoid. The anisotropy decay of an ellipsoid of revolution can display up to three correlation times, which are func-

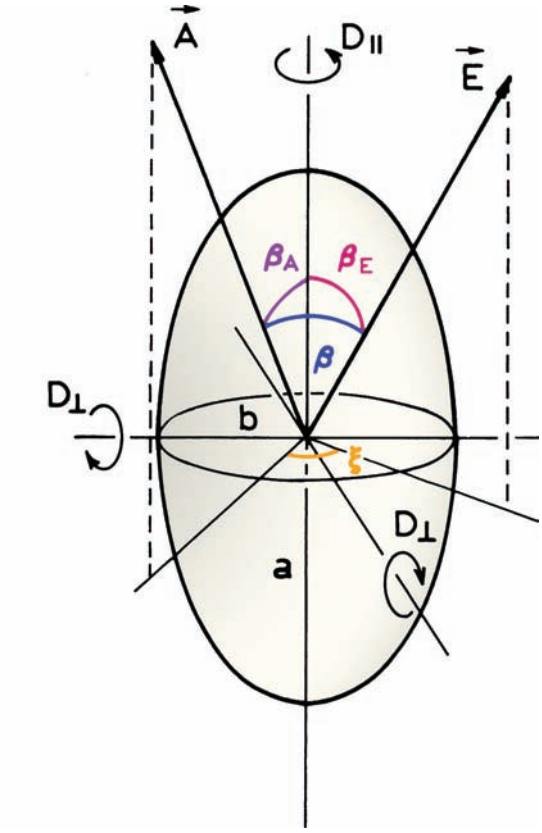

Figure 12.12. Prolate ellipsoid of revolution. $\vec{A}$ and $\vec{E}$ are the directions of the absorption and emission transition moments, respectively. Revised and reprinted with permission from [4]. Copyright © 1985, Academic Press, Inc.

tions of the two rotational rates ($D_{\|}$ and $D_{\perp}$). The amplitudes of the anisotropy decay depend on the orientation of the transition moments. If one of the transition moments is directed along any of the symmetry axes of the ellipsoid, then the anisotropy decay becomes a double exponential. Hence, one can expect double-exponential anisotropy decays for molecules like DPH or perylene, where the long-wavelength absorption and emission moments are directed along the long axis of the molecules.

12.4. ELLIPSOIDS OF REVOLUTION

We now describe the theory for the anisotropy decays of ellipsoids of revolution. It is important to remember that this theory assumes the ellipsoid to be rigid. In the case of a labeled protein this assumption implies no independent motion of the fluorophore within the protein. For prolate or oblate ellipsoids the anisotropy decay is expected to display three correlation times:

$$r(t) = r_1 \exp(-t/\theta_1) + r_2 \exp(-t/\theta_2) + r_3 \exp(-t/\theta_3) \quad (12.11)$$

The amplitudes decaying with each correlation time depend on the angles of the absorption (β_A) and emission (β_E) dipoles with the symmetry axis. Using the notation defined in Figure 12.12 these anisotropy amplitudes are

$$r_1 = 0.3 \sin 2\beta_A \sin 2\beta_E \cos\xi \quad (12.12)$$

$$r_2 = 0.3 \sin^2\beta_A \sin^2\beta_E \cos 2\xi \quad (12.13)$$

$$r_3 = 0.1(3\cos^2\beta_A - 1)(3\cos^2\beta_E - 1) \quad (12.14)$$

Occasionally one finds alternative forms[37–38] for r_1 and r_2:

$$r_1 = 1.2 \sin\beta_A \cos\beta_A \sin\beta_E \cos\beta_E \cos\xi \quad (12.15)$$

$$r_2 = 0.3 \sin^2\beta_A \sin^2\beta_E \cos 2\xi \quad (12.16)$$

The fundamental anisotropy is given as usual by

$$r_0 = r_1 + r_2 + r_3 = 0.2(3\cos^2\beta - 1) \quad (12.17)$$

where β is the angle between the absorption and emission transition moments. The three correlation times are determined by the two different rotational rates:

$$\theta_1 = (D_{\|} + 5D_{\perp})^{-1} \quad (12.18)$$

$$\theta_2 = (4D_{\|} + 2D_{\perp})^{-1} \quad (12.19)$$

$$\theta_3 = (6D_{\perp})^{-1} \quad (12.20)$$

Depending upon the shape of the ellipsoid of rotation, and the orientation of the transition moments, a variety of complex anisotropy decays can be predicted.[4,37]

In the previous chapter we saw that one can calculate these rotational correlation times for a spherical molecule (θ_S) based on its volume and the solution viscosity. Similar-

ly one can calculate $D_{\|}$ and $D_{\perp}$ for ellipsoids of revolution. These relative values are given by

$$\frac{D_{\|}}{D} = \frac{3\rho(\rho - S)}{2(\rho^2 - 1)} \tag{12.21}$$

$$\frac{D_{\perp}}{D} = \frac{3\rho\left[(2\rho^2 - 1)\,S - \rho\right]}{2(\rho^4 - 1)} \tag{12.22}$$

where $D = (6\theta_S)^{-1}$ is the rotational diffusion coefficient of a sphere of equivalent volume, and $\rho = a/b$ is the axial ratio. The value of ρ is >1 for a prolate ellipsoid and <1 for an oblate ellipsoid:

$$S = (\rho^2 - 1)^{-1/2}\ln\left[\rho + (\rho^2 + 1)^{1/2}\right] \quad \rho > 1 \tag{12.23}$$

$$S = (1 - \rho^2)^{-1/2}\arctan\left[(1 - \rho^2)^{1/2}/\rho\right] \quad \rho < 1 \tag{12.24}$$

These expressions are somewhat complex, and can be used to predict a variety of anisotropy decays. It is important to recognize that one does not directly measure the rotational diffusion coefficients, but rather the correlation times that are functions of the rotational rates.

12.4.1. Simplified Ellipsoids of Revolution

It is informative to describe the anisotropy decays when the absorption and/or emission transitions are directed along one of the axes. In these cases eqs. 12.11–12.24 reduce to simpler anisotropy decays, which can often be understood intuitively. Suppose the fluorophore is shaped like DPH, and both transition moments are aligned with the long axis (Figure 12.13, top). In this case r_1 and r_2 are zero (eqs. 12.12 and 12.13), and $r_3 = 0.4$. Hence the anisotropy decays as follows:

$$r(t) = 0.4\,\exp(-6D_{\perp}t) \tag{12.25}$$

where the correlation time is $\theta_3 = (6D_{\perp})^{-1}$. This result supports the usual assumption that DPH behaves as an isotropic rotator. DPH is not actually on isotropic rotation. However, rotation of DPH around its long axes ($D_{\|}$) does not displace the colinear transition moments, and thus does not decrease the anisotropy. Only the rotation that displaces the moments ($D_{\perp}$) results in depolarization. For this reason the anisotropy of DPH in a homogeneous solution decays with a single correlation time.

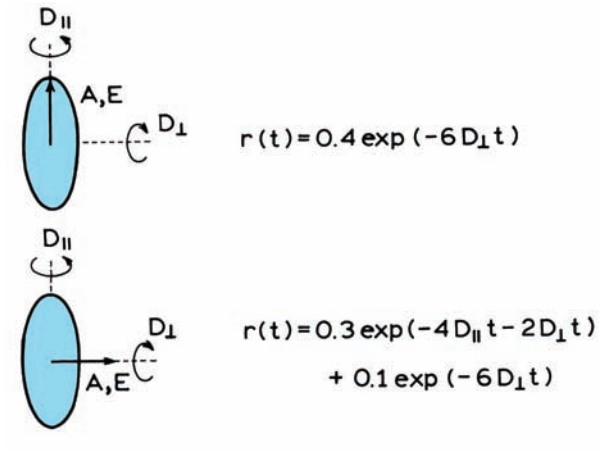

Figure 12.13. Anisotropy decays of prolate ellipsoids of revolution.

The results will be different for the same prolate ellipsoid if both transition moments are perpendicular to the long axis. In this case the anisotropy decays with two correlation times (Figure 12.13, bottom). The anisotropy decay is more rapid than in the previous case because the faster rotation about the long axis ($D_{\|}$) displaces the transition moments. This results in a rapid randomization about the long axis. At longer times the slower rotation ($D_{\perp}$) will result in complete depolarization.

The theory can also be used to predict the anisotropy decays of disk-like oblate ellipsoids (Figure 12.14). For such molecules the transitions are almost always within the plane of the ring. For colinear transitions in an oblate ellip-

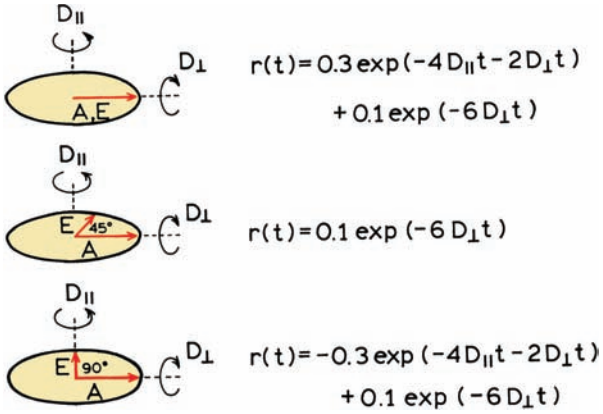

Figure 12.14. Anisotropy decays of oblate ellipsoids of revolution.

soid the anisotropy decay has the same form as that for a prolate ellipsoid with transitions normal to the long axis. The anisotropy decay is initially dominated by the faster in-plane rotation, and at later times by the slower out-of-plane rotation.

It is instructive to consider the anisotropy decays of oblate ellipsoids when the absorption and emission transitions moments are not colinear ($\beta \neq 0$). Nonzero angles occur in many fluorophores, including indole and perylene. Suppose the transition moments are within the plane and displaced by 90° ($\beta = 90°$). To be more explicit, $\beta_A = \beta_E = 90°$ and $\beta = \xi = 90°$. In this case the anisotropy decay displays positive and negative amplitudes:

$$r(t) = -0.3\exp(-4D_{\parallel}t - 2D_{\perp}t) + 0.1\exp(-6D_{\perp}t) \quad (12.26)$$

From this expression one can see that the faster in-plane rotation has a larger absolute amplitude and dominates the anisotropy decay at early times. In fact, the anisotropy can become positive prior to decaying to zero. Such behavior has been observed for perylene.

Now consider excitation when $\beta = 45°$, with $\beta_A = \beta_E = 90°$. In this case the anisotropy decay is given by

$$r(t) = 0.1\exp(-6D_{\perp}t) \quad (12.27)$$

This means that excitation at a wavelength where $r_0 = 0.1$ results in measurement of the out-of-plane rotation. When $\beta = 45°$ the excitation is randomized in the plane of the fluorophore, so the in-plane rotation has no further effects.

And finally, consider excitation with $\beta = 54.7°$, $r_0 = 0$. For this condition $r(t)$ remains zero at all times if one of the transitions is aligned with one of the axes. However, if the transitions make nonzero angles with the axes, then $r(t)$ can be nonzero at intermediate times, even with $r_0 = 0$.

An important aspect of these anisotropy decays (Figures 12.13 and 12.14) is that the correlation times are independent of r_0, but that the amplitudes (r_1, r_2, and r_3) depend on the excitation wavelength or the angles between the transition moments and the axes of the ellipsoid. This provides the opportunity for global analysis based on the anisotropy decays measured using multiple excitation wavelengths. At each excitation wavelength (or r_0 value) there will be different relative contributions of each correlation time to the anisotropy decay. However, the correlation times will be independent of excitation wavelength. By global analysis of the data, with the correlation times constrained to the same for all excitation wavelengths, one can obtain improved resolution of the multi-exponential anisotropy decay.

It is valuable to understand the origin of β values which are not equal to 0 or 90°. Individuals trained in molecular photophysics may expect the electronic transitions of perylene to be directed along the symmetry axes. For this reason the only expected values of β for perylene are 0 or 90° for the two in-plane transitions, corresponding to r_0 values of 0.40 or –0.20, respectively. However, perylene and many other fluorophores display intermediate values of β and r_0 between 0.40 and –0.20. Intermediate values of r_0 probably represent a mixture of the two electronic transitions, the relative proportion of which depends on the excitation wavelength. We describe such mixed transitions as due to a single apparent value of β for a single transition.

12.4.2. Intuitive Description of Rotational Diffusion of an Oblate Ellipsoid

The special cases described above can be understood intuitively by considering rotational diffusion of perylene. Assume perylene is excited in its long-wavelength absorption band where r_0 is near 0.4. The excited-state population will initially be aligned along the vertical or z-axis (Figure 12.15). Rotation of perylene about its symmetry axis (normal to the plane) will displace the transition moments and result in depolarization. Similarly, one of the out-of-plane rotations will displace the transition moments. This intuitive result agrees with Figure 12.14 (middle panel), which indicates that for an oblate ellipsoid with $r_0 = 0.4$ both $D_{\parallel}$ and $D_{\perp}$ contribute to the anisotropy decay.

Now consider excitation of perylene with $r_0 = -0.2$, $\beta = 90°$. Initially, neither out-of-plane rotation displaces the emission moment, so the only active depolarizing rotation is the in-plane rotation. (Recall the excited state population is symmetrical around the z-axis). Once the molecule has undergone in-plane rotation then the out-of-plane rotation displaces the emission moment. These motions result in the anisotropy decay described by eq. 12.26.

And, finally, consider excitation with $\beta = 45°$ or $r_0 = 0.10$. In this case the excited-state population is immediately randomized around the symmetry axis of the oblate ellipsoid. Hence only the out-of-plane rotations can further depolarize the emission, which is in agreement with eq. 12.27.

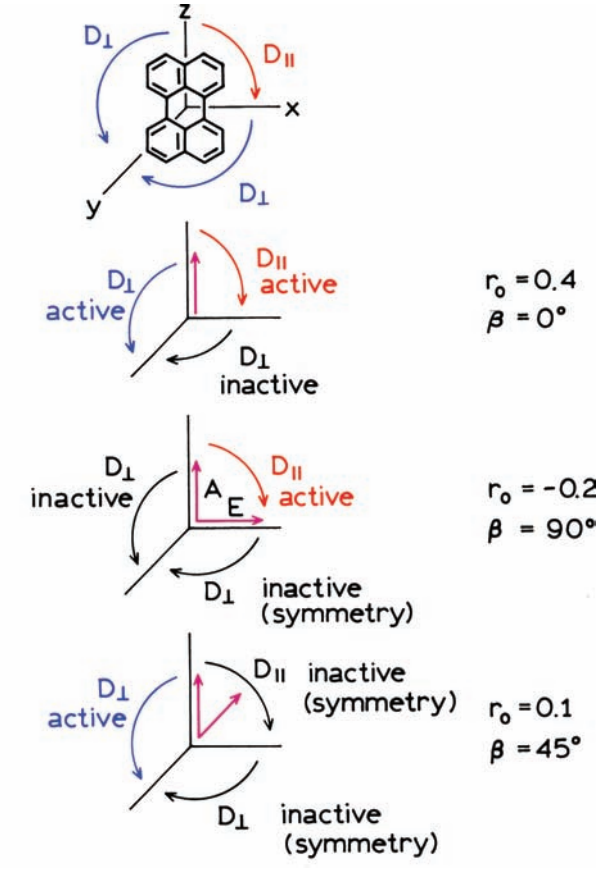

Figure 12.15. Rotational motions of an oblate ellipsoid.

12.4.3. Rotational Correlation Times for Ellipsoids of Revolution

It is interesting to see how the shape of an ellipsoid affects the correlation times. Some correlation times are summarized in Table 12.1. These values are shown as the ratio of the rotational correlation times for the ellipsoid to that expected for a sphere of equivalent volume.[39] The correlation times are quite different for prolate and oblate ellipsoids. For prolate ellipsoids the three correlation times are all different in magnitude, and can be much larger than that for an equivalent sphere. For the prolate ellipsoids one correlation time (θ_3) increases dramatically as the axial ratio increases. This is understandable because a long rigid rod is expected to diffuse slowly in directions which displace the long axis. This correlation time ($\theta_3 = (6D_\perp)^{-1}$) is determined by the rotation that displaces the long axis of the prolate ellipsoid. For a prolate ellipsoid all three correlation times can be distinct for large axial ratios. The ability to detect these correlation times depends on the amplitudes, which depend on the angles with respect to the symmetry axis. For the oblate ellipsoids the three correlation times are all similar in magnitude. Hence it would be difficult to distinguish an oblate ellipsoid from a sphere, assuming that the oblate ellipsoid displayed hydrodynamic rotation. However, small oblate molecules often display slip diffusion, which results in faster in-plane rotations.

Some fluorophores display r_0 values near 0.4, which indicates that the absorption and emission moments are colinear. In this case eqs. 12.12 and 12.13 can be simplified further. Using $\beta_A = \beta_E = \beta_T$ and $\xi = 0$ one finds

$$r_1 = 0.3 \sin^2 2\beta_T \tag{12.28}$$

$$r_2 = 0.3 \sin^4 \beta_T \tag{12.29}$$

$$r_3 = 0.1(3\cos^2 \beta_T - 1)^2 \tag{12.30}$$

where β_T is the angle formed by the transition moments with the symmetry axis of the ellipsoid.

Because of the complexity of the equations relating shape to the anisotropy decays, it is useful to have some specific examples. Rotational correlation times for prolate ellipsoids are summarized in Table 12.2. These correlation times are calculated for proteins with $\bar{\upsilon} = 0.75$ ml/g and for

Table 12.1. Rotational Correlation Times of Ellipsoid of Revolution[a]

Prolate				Oblate			
ρ	θ_1/θ_S	θ_2/θ_S	θ_3/θ_S	ρ^{-1}	θ_1/θ_S	θ_2/θ_S	θ_3/θ_S
1	1.0	1.0	1.0	1	1.0	1.0	1.0
2	1.32	0.95	1.50	2	1.17	1.49	1.13
5	2.41	0.98	4.64	5	2.30	2.51	2.24
10	3.25	0.99	13.37	10	4.38	4.61	4.30
20	3.73	0.99	41.82	20	8.60	8.85	8.52

[a]From [39]. $\theta_1 = (D_\parallel + 5D_\perp)^{-1}$, $\theta_2 = (4D_\parallel + 2D_\perp)^{-1}$, $\theta_3 = (6D_\perp)^{-1}$.

Table 12.2. Rotational Correlation Times for Prolate Ellipsoids of Revolution[a]

	MW = 10,000							
	θ_1 (ns)		θ_2 (ns)		θ_3 (ns)		θ_H (ns)	
ρ	$h = 0$	$h = 0.2$	$h = 0$	$h = 0.2$	$h = 0$	$h = 0.2$	$h = 0$	$h = 0.2$
1.5	3.46	4.38	2.94	3.72	3.68	4.66	3.27	4.14
2	4.05	5.13	2.93	3.71	4.63	5.87	3.59	4.55
3	5.31	6.72	2.97	3.77	7.18	9.11	4.21	5.34
5	7.40	9.36	3.03	3.83	14.2	18.0	5.00	6.31
10	10.03	12.67	3.06	3.88	41.7	52.1	5.69	7.24\
	MW = 25,000							
1.5	8.66	10.96	7.34	9.31	9.21	11.65	8.16	10.37
2	10.11	12.79	7.33	9.29	11.57	14.62	8.96	11.36
3	13.2	16.8	7.43	9.42	17.9	22.8	10.54	13.25
5	18.4	23.4	7.56	9.60	35.4	45.0	12.36	15.96
10	25.1	31.6	7.65	9.71	104.2	128.2	14.23	23.19
	MW = 50,000							
1.5	17.4	21.8	14.7	18.5	18.5	23.1	16.3	20.6
2	20.2	25.5	14.7	18.4	23.1	29.2	17.8	22.4
3	26.7	33.3	15.0	18.7	36.2	45.0	21.0	26.7
5	37.3	46.1	15.2	19.0	72.4	87.7	24.8	31.2
10	50.2	64.1	15.3	19.4	208.3	277.8	28.5	36.2
	MW = 100,000							
1.5	34.7	43.4	29.3	36.7	37.0	46.3	32.6	41.8
2	40.5	50.2	29.4	36.5	46.3	57.4	36.9	44.5
3	53.4	65.3	29.9	37.0	72.4	87.7	42.2	52.1
5	73.0	94.3	30.1	38.1	138.9	185.2	49.5	63.3
10	100.0	128.2	30.4	38.7	416.7	555.5	56.6	72.3
	MW = 500,000							
1.5	173.9	217.9	147.1	185.2	185.2	231.5	163.4	205.8
2	202.4	255.1	147.0	184.5	231.5	292.4	177.9	225.4
3	267.4	333.3	149.7	187.3	362.3	450.5	209.6	267.7
5	373.1	460.8	152.0	190.1	724.6	877.2	248.0	332.0
0	502.5	641.0	153.4	193.8	2083.3	2777.8	285.1	375.4

[a] $\theta_1 = (D_\parallel + 5D_\perp)^{-1}$, $\theta_2 = (4D_\parallel + 2D_\perp)^{-1}$, $\theta_3 = (6D_\perp)^{-1}$. $D_\perp/D$ from eq. 12.21 and $D_\parallel/D$ from eq. 12.21, S from eq. 12.23, $\bar{\upsilon} = 0.75$.

a hydration of $h = 0$ or $h = 0.2$ ml/g. Values are not listed for oblate ellipsoids since most non-spherical proteins seem to be elongated rather than flattened. Of course, all the correlation times increases with increasing molecular weight. Two of the correlation times (θ_1 and θ_3) increase dramatically as the axial ratio increases. The other correlation time (θ_2) is relatively independent of shape.

It is useful to visualize how the three correlation times depend on the axial ratio. This dependence is shown in Figure 12.16 for a prolate ellipsoid of revolution. The chosen parameters MW = 10,000, $\sqrt{\upsilon} = 0.75$, $\bar{\upsilon} = 0.75$ ml/g, and $h = 0.2$ ml/g were selected to represent a small protein. One of the correlation times (θ_3) increases progressively as the axial ratio increases. The other two correlation times (θ_1 and θ_2) reach limiting values at large axial ratios. This occurs because these correlation times contain $D_\parallel$, which stays relatively constant as ρ increases. It is interesting to note that θ_2 actually decreases as ρ increases from 1 to 3.

Also shown in Table 12.2 are the harmonic mean correlation times (θ_H). Calculation of θ_H is somewhat complicated because it depends on the value of r_0 and the orientation of the transition moments relative to the ellipsoid axis. The values in Table 12.2 were calculated using

$$\frac{1}{\theta_H} = \frac{0.4}{\theta_1} + \frac{0.4}{\theta_2} + \frac{0.2}{\theta_3} \qquad (12.31)$$

This definition of θ_H is appropriate when the absorption and emission transition moments are randomly oriented with respect to the principal axes.[36]

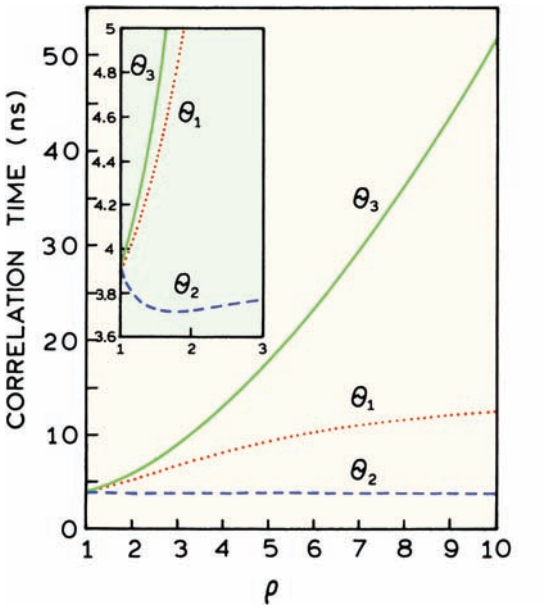

Figure 12.16. Correlation time for a prolate ellipsoid of revolution at various axial ratios (ρ), η = 1 cP, $\theta_1 = (D_{\|} + 5D_{\perp})^{-1}$, $\theta_2 = (4D_{\|} + 2D_{\perp})^{-1}$, $\theta_3 = (6D_{\perp})^{-1}$. MW = 10,000, h = 0.2 ml/g and $\bar{\upsilon}$ = 0.75 ml/g.

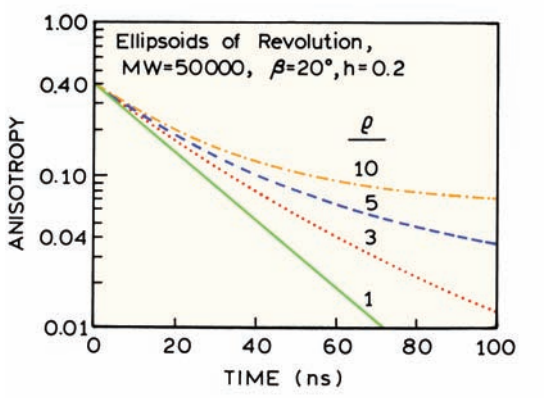

Figure 12.17. Simulated anisotropy decays for a protein (MW = 50 kD) shaped as a prolate ellipsoid of revolution with various axial ratios (ρ). For these simulations we assumed $\bar{\upsilon}$ = 0.75 ml/g, h = 0.2 ml/g, and β = 20°.

The form of an anisotropy decay depends on the axial ratio. The anisotropy decays were simulated using the assumption r_0 = 0.4 (eqs. 12.28–12.30) and various axial ratios (Figure 12.17). For these decays the transition moments were assumed to make an angle of 20° relative to the symmetry axis of the prolate ellipsoid. The anisotropy decays became visually different from a single exponential as the axial ratio exceeded 2. This change in the shape of an anisotropy decay is the basis for determining the shapes of proteins from the time-resolved anisotropies.

12.4.4. Stick-versus-Slip Rotational Diffusion

The theory described above for rotation of ellipsoids applies only to the "stick" condition. The term "stick boundary conditions" refers to rotational diffusion in which the first solvent layer moves with the rotating species, so that rotation is governed by the viscosity of the solvent. Macromolecules and most fluorophores in polar solvents are well described by stick diffusion. However, small molecules in nonpolar solvents can often display slip-rotational diffusion.[40–46] As an example, perylene in a solvent like hexane can rotate in plane without significant displacement of solvent. When this occurs the molecule rotates as if it were in a vacuum, and not affected by solvent viscosity. The theory of slip-rotational diffusion is rather complex, and the results are often presented numerically.[47–48] The important point is that the possibility of slip diffusion results in a failure of the theory described above to predict the correlation times of non-spherical molecules. Stated alternatively, one can recover multiple correlation times for small non-spherical molecules, but these values cannot always be interpreted in terms of the correlation times predicted from the hydrodynamic theory (eqs. 12.11–12.24).

12.5. COMPLETE THEORY FOR ROTATIONAL DIFFUSION OF ELLIPSOIDS

In the preceding sections we described the rotational behavior of ellipsoids with transitions directed along one of the symmetry axes. Although not frequently used, it is useful to have the complete expression for an ellipsoid with three nonequivalent axes and without restricting one of the transitions to be on an axis (Figure 12.10, left). In this case the anisotropy decays with five apparent correlation times:[30,36,39]

$$r(t) = \frac{6}{5}\sum_{i=1}^{3} C_i \exp(-t/\theta_i) + [(F+G)/4]\exp[-(6D-2\Delta)t] + [(F-G)/4]\exp[-(6D+2\Delta)t] \quad (12.32)$$

In this expression D is the mean rotational diffusion coefficient:

$$D = \frac{1}{3}(D_1 + D_2 + D_3) \tag{12.33}$$

and

$$\Delta = (D_1^2 + D_2^2 + D_3^2 - D_1D_2 - D_1D_3 - D_2D_3)^{1/2} \tag{12.34}$$

The directions of the transition moments in the ellipsoid (Figure 12.12) are defined by the cosine of the angles between the absorption transitions and the three axes (α_1, α_2 and α_3) and between the emission transitions (ε_1, ε_2, and ε_3) and the three axes. The values of C_i are given by

$$C_i = \alpha_j\alpha_k\varepsilon_j\varepsilon_k \tag{12.35}$$

with ijk = 123, 231, or 312. The other quantities in eq. 12.32 are defined by

$$C_i = \alpha_j\alpha_k\varepsilon_j\varepsilon_k \tag{12.36}$$

$$F = \sum_{i=1}^{3} \alpha_i^2\varepsilon_i^2 - 1/3 \tag{12.37}$$

$$G\Delta = \sum_{i=1}^{3} D_i(\alpha_i^2\varepsilon_i^2 + \alpha_j^2\varepsilon_k^2 + \alpha_k^2\varepsilon_j^2) - D \tag{12.38}$$

where $i \neq k$.

In the limiting case of spherical symmetry, with $D_1 = D_2 = D_2 = D$, eq. 12.32 reduces to a single correlation time with $\theta = (6D)^{-1}$. For ellipsoids of revolution these equations (12.32 to 12.38) reduce to those given in Section 12.4.

12.6. ANISOTROPIC ROTATIONAL DIFFUSION

12.6.1. Time-Domain Studies

It is difficult to detect the presence of anisotropic rotation.[49–53] In one report[53] the anisotropy decay of 9,10-dimethylanthracene (DMA) was measured in a viscous nonpolar solvent. The sample was excited at 401 nm using the 0.5-ns pulses available from a synchrotron. The solvent was glycerol tripropanoate, which at -38.7°C had a viscosity of 11 poise. Under these conditions the mean correlation time was 10 ns. The experimental anisotropy decay could not be fit to a single correlation time (Figure 12.18), but the data were well fit using two correlation times (not shown). The presence of two correlation times is consistent with DMA being an ellipsoid of revolution, but the recovered diffusion coefficients did not agree with those predicted from the hydrodynamic theory for ellipsoids. This failure was assigned to the presence of partial slip diffusion. The overall behavior of DMA appeared to be intermediate between the slip and stick diffusion limits.

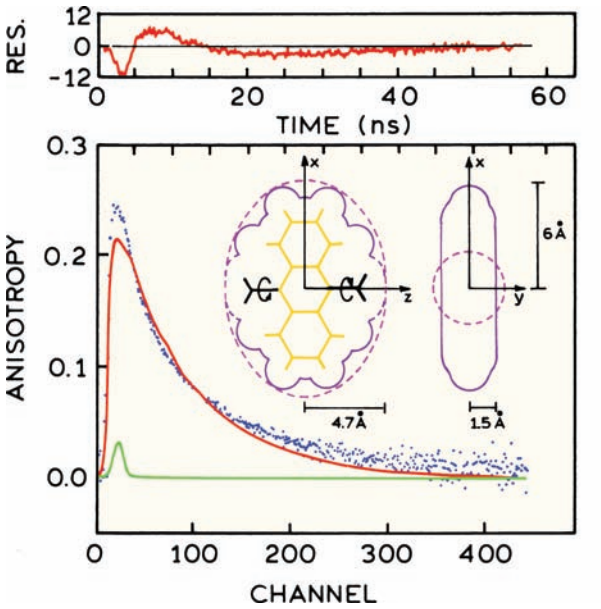

Figure 12.18. Time-domain anisotropy decay of 9,10-dimethylanthracene in glycerol tripropanoate (tripropionin) at –38.4°C. Excitation at 401 nm was obtained as 0.5-ns pulse from the LURE-ACO synchrotron, Orsay, France. The solid line shows the single correlation time fit. Revised and reprinted with permission from [53]. Copyright © 1985, American Chemical Society.

Perylene has been widely studied as an anisotropic rotation. When excited in its long-wavelength absorption band the anisotropy decay is a double exponential, but this can be difficult to detect from the time-resolved data. The use of a shorter excitation wavelength results in a definitive observation.[49] At this wavelength the absorption and emission transition moments are nearly perpendicular, and the time-zero anisotropy is –0.14. For a spherical molecule the anisotropy is expected to decay from –0.14 to zero with a single correlation time. However, the anisotropy of perylene increases to values above zero and then decays to zero (Figure 12.19). This behavior can be understood in terms of the different rotational motions of perylene.

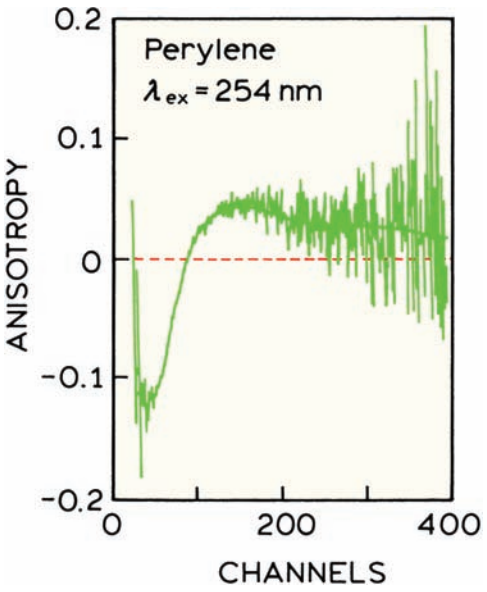

Figure 12.19. Anisotropy decay of perylene in glycerol at 30°C. Excitation at 254 nm where r_0 = –0.14. The data were fit as $r(t)$ = 0.1 exp(–t/17 ns) – 0.24 exp(–t/2.7 ns). Revised and reprinted with permission from [49]. Copyright © 1981, American Institute of Physics.

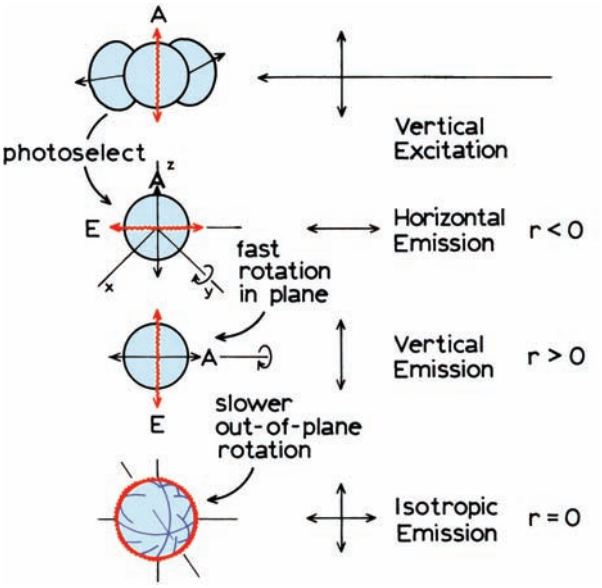

Figure 12.20. Effect of faster in-plane rotations on the anisotropy decay of perylene with r_0 = –0.2. Revised and reprinted with permission from [37], Academic Press Inc.

An intuitive description of the unusual perylene anisotropy decay is shown in Figure 12.20. When excited at a wavelength with r_0 = –0.2 the emission moments are symmetrically distributed in the laboratory x–y plane, and the horizontal intensity is greater than the vertical intensity (r_0 < 0). Because the in-plane rotation is more rapid than the out of plane rotation, the effect at short times is to rotate the emission dipoles out of the x–y plane toward the vertical axis. This results in transient anisotropy values above zero (Figure 12.19). At longer times the slower out-of-plane motions contribute to depolarization, and the anisotropy decays to zero (Figure 12.20).

12.6.2. Frequency-Domain Studies of Anisotropic Rotational Diffusion

Anisotropic rotational diffusion can be studied using frequency-domain methods. In fact, the earliest reports on the anisotropic rotation of fluorophores were performed using fixed-frequency phase-modulation fluorometers.[54–56] At that time the phase-modulation instruments operated at only one or two fixed frequencies. Hence it was not possible to recover the anisotropy decay law. The experiments were performed by measuring the differential polarized phase angles (Δ_ω) as the temperature was varied. It is relatively simple to predict the maximum value of Δ_ω for known values of the lifetime and fundamental anisotropy. For an isotropic rotator the predicted value of Δ_ω is given by

$$\tan \Delta_\omega = \frac{(2D\tau)\,\omega\tau r_0}{\frac{1}{9}m_0(1+\omega^2\tau^2) + [(2D\tau)/3](2+r_0) + (2D\tau)^2} \tag{12.39}$$

where $m_0 = (1 + 2r_0)(1 - r_0)$. The value of tan Δ_ω is a function of the rotational rate (D), r_0, τ, and ω. The maximum value of tan Δ_ω is given by

$$\tan \Delta_\omega^{\max} = \frac{3\omega\tau r_0}{(2+r_0) + 2[m_0(1+\omega^2\tau^2)]^{1/2}} \tag{12.40}$$

and is independent of the rotational rate. We note that these expressions are only valid for an isotropic rotor with a single fluorescence lifetime. The maximum differential tangent depends only on τ, r_0, and ω. If there is more than one rotational rate the maximum value of tan Δ is decreased.[54]

Anisotropic rotation of perylene was detected by measurements of the temperature-dependent values of tan Δ, measured at a single modulator-frequency.[55] The values of tan Δ are only nonzero in the temperature range where rotational diffusion is on a timescale comparable to the lifetime.

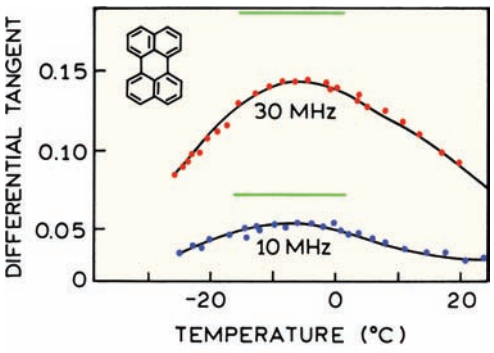

Figure 12.21. Differential polarized phase angles of perylene in propylene glycol. The horizontal solid bars show the theoretical maximum values for tan Δ_ω with isotropic rotation. Revised and reprinted from [55]. Copyright © 1977, American Institute of Physics.

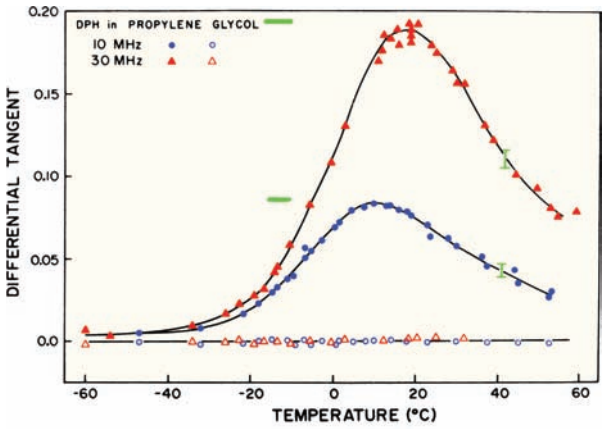

Figure 12.22. Temperature dependence of the differential polarized phase angles of DPH in propylene glycol. The solid bars show the maximum values of tan Δ_ω for isotropic rotation. The open symbols are the values of tan Δ_ω measured with horizontally polarized excitation. Reprinted with permission from [57]. Copyright © 1979, American Chemical Society.

At very high or low temperatures tan $\Delta = 0$. Figure 12.21 shows the temperature-dependent data for perylene in propylene glycol. The maximum values of tan Δ are significantly smaller than the values predicted using eq. 12.40. Molecules like DPH, which are not spheres but do display a single rotational rate, display tan Δ_ω^{max} values that agree with the calculated values (Figure 12.22). The single-frequency data for perylene do not allow determination of the anisotropy decay parameters. The presence of anisotropic rotations in perylene were also detected by early studies with a variable frequency instruments, which indicated the correlation time for perylene was smaller than predicted based on its size.[58]

Frequency-domain measurements can be used to resolve complex anisotropy decays.[59] The resolution of the anisotropy decays is rather good, which is probably the result of direct measurement of the difference between the polarized components of the decay. In the frequency domain these differences are measured directly. In the time domain the anisotropy decay is calculated from the two independently measured quantities, $I_{\|}(t)$ and $I_{\perp}(t)$. Additionally, there are two observable quantities in the frequency domain—Δ_ω and Λ_ω—which provides better resolution than the use of either quantity alone.

Resolution of anisotropic rotational diffusion using FD measurements is illustrated by data for two fluorophores: fluorescein and perylene. Frequency-domain anisotropy data for fluorescein are shown in Figure 12.23. This figure is visually similar to Figure 12.21, but the *x*-axis on Figure 12.23 is frequency and not temperature. These frequency-domain data are almost perfectly fit using a single correlation time, indicating that fluorescein behaves like an isotropic rotator.[60] Such behavior is expected for polar fluorophores in polar solvents. It appears that hydrogen bonding interactions decrease slip diffusion, and result in more isotropic rotations.

Rather different results were obtained for perylene (Figure 12.24). The frequency-domain data could not be fit

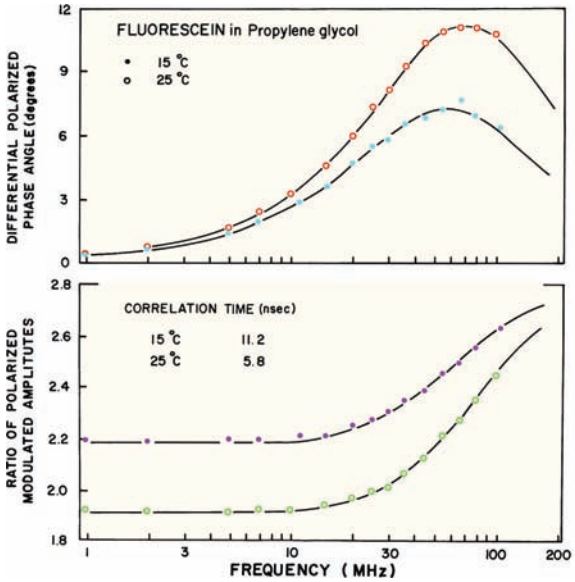

Figure 12.23. Frequency-domain anisotropy decay of fluorescein in propylene glycol. The solid lines show the best single correlation time fits. The lifetime of fluorescein was 3.7 ns at 15 and 25°C. Revised and reprinted with permission from [60]. Copyright © 1985, American Chemical Society.

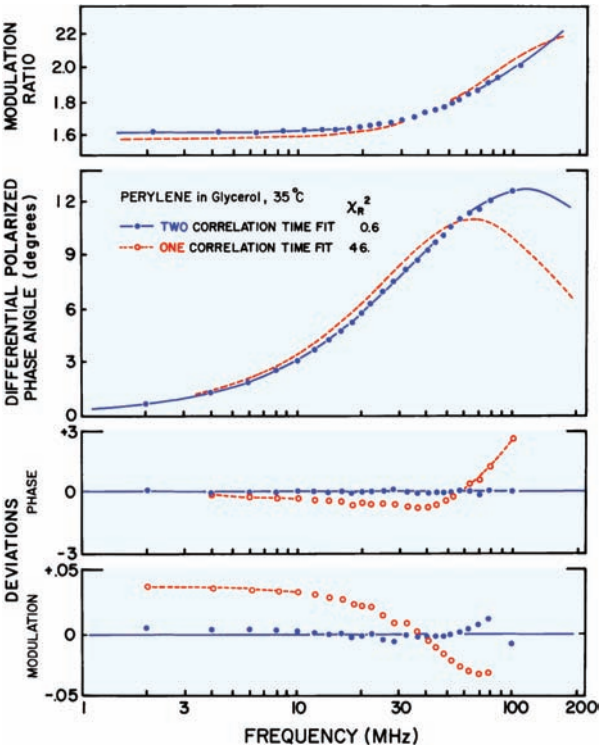

Figure 12.24. Frequency-domain anisotropy decay of perylene in glycerol at 35°C. The lifetime was 4.8 ns. Reprinted from [61]. Copyright © 1985, with permission from Elsevier Science.

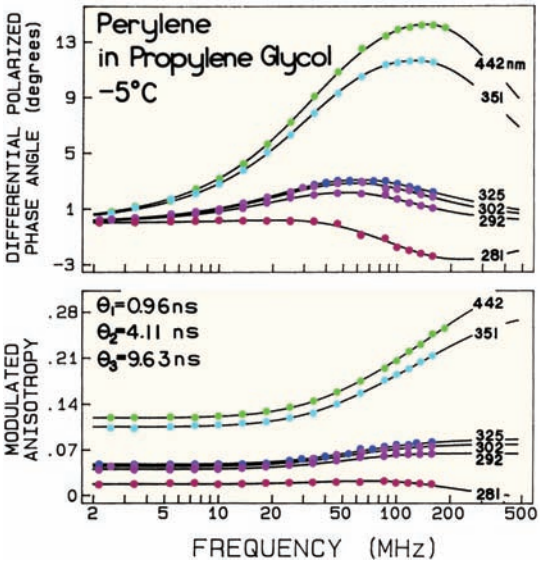

Figure 12.25. Frequency-domain anisotropy decays of perylene for various excitation wavelengths. From [65].

to a single correlation time (dashed), but these data were well fit using two correlation times.[61] The multi-exponential anisotropy decay analysis yielded amplitudes of r_{01} = 0.17 and r_{02} = 0.18, with correlation times of 1.5 and 10.8 ns. This ratio of correlation times is comparable to that recovered from the TD data.[49] The 80-fold decrease in χ_R^2 for the two-correlation time fit as compared to the one-correlation time fit, and the large and systematic deviation for the one-correlation time fit, indicate that complex anisotropy decays can be recovered from the FD data.

12.7. GLOBAL ANISOTROPY DECAY ANALYSIS

12.7.1. Global Analysis with Multi-Wavelength Excitation

The use of multiple excitation wavelengths provides a useful method for improving the resolution of closely spaced correlation times. For a rigid non-spherical molecule, different values of r_0 are expected to yield different anisotropy amplitudes, but the same correlation times will remain the same. The contributions of diffusion coefficients are different for different values of r_0 (eqs. 12.11–12.20). The use of different excitation wavelengths allows each rotational rate to contribute differently to the data.[62–64]

The concept of using different r_0 values is illustrated by perylene (Figure 12.25). A wide range of r_0 values are available using perylene with different excitation wavelengths (Figure 12.34, below). For longer excitation wavelengths (351 and 442 nm) the fundamental anisotropy of perylene is near 0.35. For excitation between 292 and 325 nm the fundamental anisotropy is near 0.07, and for excitation at 281 the anisotropy is slightly below zero. Figure 12.25 shows that the frequency of the maximum differential phase angle depends on excitation wavelength. If there were a single rotational correlation time the curves would be proportional to r_0, but the shape would be unchanged. The shape changes because of the multiple rotational rates, and their different contributions at each excitation wavelength.

The wavelength-dependent shifts in the differential polarized phase curves can be understood in terms of the contribution of various rotations to the anisotropy decay. As reasoned in Figures 12.14 and 12.15, both the in-plane and out-of-plane rotations are expected to contribute where r_0 = 0.4. Hence the data for 351 and 442 nm excitation represent a weighted average of $D_{\|}$ and $D_{\perp}$. For r_0 values near –0.2 one expects the in-plane rotation to be dominant (Figure 12.20). This effect can be seen in the data for 281-nm excitation, for which the maximum value of Δ_ω (absolute value) is shifted toward higher modulation frequencies. And, final-

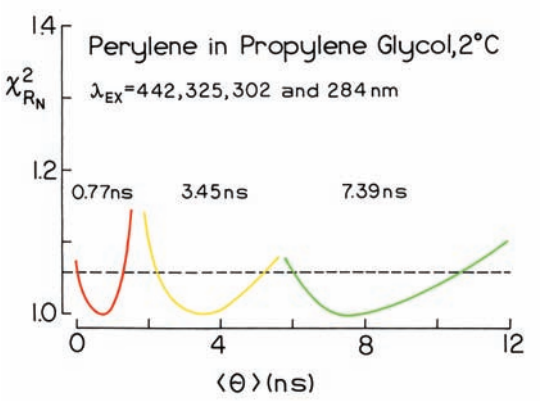

Figure 12.26. χ_R^2 surfaces for the three correlation times found for perylene. From [65].

ly, for r_0 values near 0.1 one expects the out-of-plane rotation to dominate the anisotropy decay. These slower motions display a maximum value of Δ_ω of lower modulation frequencies.

Global analysis of the frequency-domain data is performed assuming the correlation times are independent of excitation wavelength, and that the amplitudes are dependent on wavelength. Under these assumptions the value of χ_R^2 is calculated using an expanded form of eq. 11.34, where the sum extends over the excitation wavelengths. The changes in shape of Δ_ω allow highly detailed resolution of an anisotropy decay using global analysis. In fact, the data allowed recovery of three rotational correlation times. The fact that the three correlation times were needed to explain the data was demonstrated for the χ_R^2 surfaces (Figure 12.26). The presence of three correlation times for perylene is somewhat surprising because the transitions of perylene are along its long and short axes (Figure 12.35, below), and it is shaped like an oblate ellipsoid. Hence, only two correlation times are expected. The recovered correlation times and amplitudes do not seem to fit any reasonable hydrodynamic shape.[65] It appears that perylene displays partial slip diffusion and thus an anisotropy decay different from that predicted from the hydrodynamic model.

12.7.2. Global Anisotropy Decay Analysis with Collisional Quenching

As shown in Chapter 10 (eq. 10.43), the steady-state anisotropy is the average value of the anisotropy decay averaged over the intensity decay of the sample. If the sample displays several correlation times, eq. 10.49 indicates that their contributions to the anisotropy would be different if the lifetime was changed. This is possible using energy transfer or collisional quenching.[66–68] Consider a sample with a lifetime of 4 ns and a correlation time of 4.0 or 0.4 ns (Figure 12.27). The information about the anisotropy decay is contained in the difference between the parallel ($I_\parallel$) and perpendicular ($I_\perp$) components of the emission (Figure 12.27, left). For the 4-ns correlation time (dashed lines), the

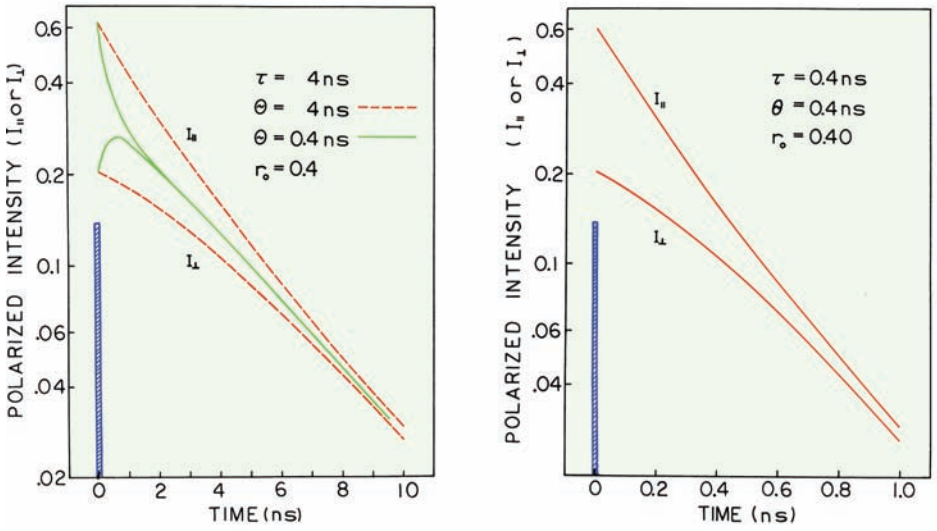

Figure 12.27. Simulated anisotropy decays for unquenched and quenched decays. Left: Unquenched decay with τ = 4 ns and θ = 4 (dashed lines), or 0.4 ns (solid lines). Right: Quenched decay with τ = 0.4 ns and θ = 0.4 ns. r_0 is 0.4 for both decays. Reprinted with permission from [69]. Copyright © 1987, Biophysical Society.

difference persists throughout the duration of the emission, and all the emitted photons aid in recovering the anisotropy decay. Now suppose the correlation time is 400 ps (solid lines). The polarized components are essentially equal after 1 ns, and the photons detected after this time do not aid in recovering the anisotropy decay. However, the emitted photons all contributed to the emission and to the acquisition time. Because the acquisition times must be finite, it is difficult to collect data adequate to determine the picosecond correlation time because most of the observed photons will not contain information about the correlation time. Now consider the effect of decreasing the decay time to a subnanosecond value of 0.4 ns by quenching (Figure 12.27, right). Because of the shorter lifetime a larger fraction of the emission contains information on the 0.4-ns correlation time. Hence information on the faster process is increased by measurement of the quenched samples.

For determination of a single short correlation time, analysis of data from the most quenched sample is adequate. However, the usual goal is to improve resolution of the entire anisotropy decay. This can be accomplished by simultaneous analysis of data from the unquenched and several quenched samples. The data from the unquenched sample contributes most to determination of the longer correlation times, and the data from the quenched sample contributes to resolution of the faster motions.

12.7.3. Application of Quenching to Protein Anisotropy Decays

The use of global analysis with quenching is useful for studies of complex anisotropy decays from proteins. This is because the correlation times for segmental motions and overall rotations of a protein are usually quite different in magnitude. The correlation times of a rigid rotor are usually similar in magnitude, so that quenching is less useful.

The value of quenching can be seen from the simulated frequency-domain data (Figure 12.28). The unquenched lifetime was again assumed to be 4 ns. The correlation times were assumed to be 10 ns for overall rotation and 0.1 ns for the segmental motions. To be comparable with the data found for the proteins the fundamental anisotropy (r_0) was 0.30, and the anisotropy amplitude of the segmental motion was taken as 0.07. Assume that the lifetime is reduced to 2.0 or 0.5 ns by quenching. In practice the decays may become more heterogeneous in the presence of quenching due to transient effects in diffusion, but this is not important for the simulations.

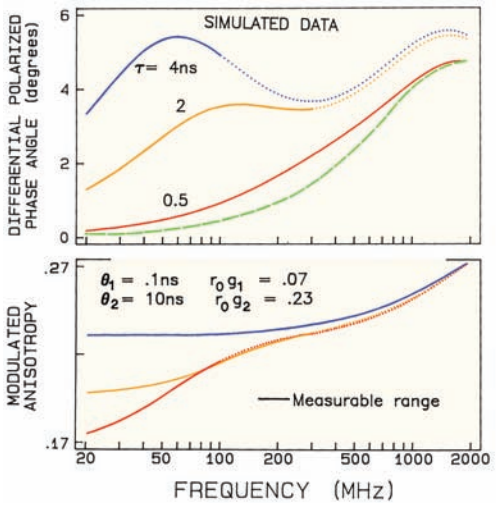

Figure 12.28. Simulated frequency-domain anisotropy data. The simulated correlation times were assumed to be 0.10 and 10.0 ns, with amplitudes of 0.07 and 0.23, respectively. Simulated data are shown for intensity decay times of 4, 2, and 0.5 ns. The solid regions of the curves indicate the measurable frequency range, where the modulation is 0.2 or larger for the intensity decay. The dashed line shows the phase values expected for the 0.1 ns correlation time, with the smaller amplitude (0.07). From [70].

The existence of two rotational motions is seen in the frequency response of the polarized emission. These motions are evident from the two peaks in the plots of differential phase angles. These peaks are due to the individual motions with correlation times of 10 and 0.1 ns. The 10-ns motion is responsible for the peak near 60 MHz. The 100-ps motion is responsible for the peak at higher frequencies (dashed line), with a maximum near 2 GHz. These are two features of the data from the quenched samples that provide increased resolution of the anisotropy decay. First, the frequency-domain data can be measured at higher frequencies for the samples with shorter decay times. This is because the emission is less demodulated with the shorter lifetimes. The solid regions of the curves show the measurable frequency range where the modulation of the emission is 20% or larger, relative to the modulation of the incident light. Based on this criterion the upper frequency limit in the absence of quenching ($\tau_0 = 4$ ns) is only 100 MHz. If the lifetime is reduced to 0.5 ns, the upper frequency limit is 2 GHz, which provides more data at frequencies characteristic of the faster motion.

Quenching also increases the information content of the modulated anisotropies (lower panel, Figure 12.28). At low frequencies the value of the modulated anisotropy is equal to the steady-state anisotropy, which is increased by

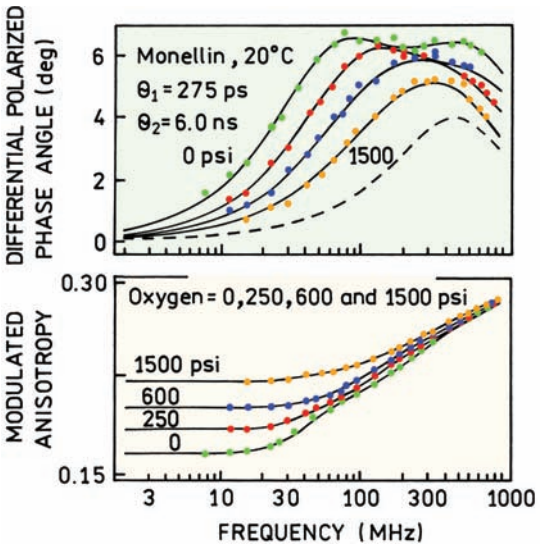

Figure 12.29. Frequency-domain anisotropy data for monellin with oxygen quenching. Data are shown for oxygen pressures of 0, 250, 600, and 1500 psi. The dashed line shows the values expected for a correlation time of 275 ps, with an amplitude of 0.075. From [70].

quenching. Once again the measurable range is extended to 2 GHz by collisional quenching. The values of r_ω for the unquenched sample increase over the frequency range from 20 to 100 MHz, which is the portion of r_ω that depends upon overall rotation of the protein. For the quenched sample the higher-frequency data begin to show a contribution from the faster motion.

An advantage of measuring a series of progressively quenched samples is that the data are differently sensitive to the two motions. The same motions determine the values of Δ_ω and Λ_ω in the quenched and the unquenched samples. However, the proportions each motion contributes are different. As the decay time is decreased by quenching, the data is shifted towards higher frequencies and the contribution of overall diffusion is decreased (Figure 12.28). These effects provide increased resolution by simultaneous analysis of the data from a series of progressively quenched samples.

The value of global anisotropy analysis using quenched samples is illustrated for monellin. This is a naturally sweet protein that contains a single-tryptophan residue. This residue is rather mobile, as seen from the two peaks in the differential phase angles near 70 and 500 MHz (Figure 12.29). As the sample is quenched by oxygen, the component due to overall rotation near 70 MHz decreases in amplitude. At the highest amounts of quenching the FD anisotropy data become dominated by the contribution of the shorter correlation time near 275 ps. Hence, one can visualize how global analysis of quenched and unquenched samples provides improved resolution of the two correlation times.

12.8. INTERCALATED FLUOROPHORES IN DNA

Many fluorophores intercalate into double-helical DNA. Some fluorophores, like ethidium bromide (EB), become more highly fluorescent when bound to DNA, allowing the emission for the DNA-bound probes to be easily detected. Consequently, there have been numerous studies of the anisotropy decays of DNA-bound probes. At first glance a DNA-bound probe seems relatively simple. Suppose the probe is located between the DNA base pairs, which is referred to as being intercalated. The anisotropy decay of such a probe is determined by its freedom within the DNA helix, and by the diffusive motions of DNA. These motions are characterized by the torsional motions around the z-axis of DNA (Figure 12.30), and by bending motions about the x-axis.

There have been theoretical reports on the anisotropy decay expected for DNA bound probes.[71–73] Unfortunately, the theory is complex in its complete form. The contribution of the torsional and bending motions of DNA depend on the orientation of the probe within the DNA helix, and

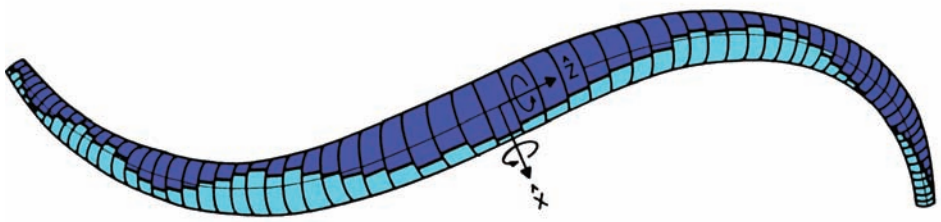

Figure 12.30. Torsional and bending motions of DNA. From [73].

the value of r_0. Also, the depolarization due to the torsional motions and bending motions occur on very different timescales. In fact, the bending motions do not make a significant contribution to the anisotropy decay of EB with its 23-ns lifetime, and $r(t)$ is dominated by torsional motions around the z-axis.

Because of the complexity of the theory, one often encounters various simplified forms. When the absorption and emission transition moments are colinear, and perpendicular to the helix axis, the anisotropy decay is given by[37]

$$r(t) = \{0.75 \exp[-\Gamma(t)] + 0.45 \exp[-\Delta(t) + \Gamma(t)] + 0.4 \exp[-\Delta(t)]\}/\{3 + \exp[-\Delta(t)]\} \quad (12.41)$$

where the twisting decay function is given by

$$\Gamma(t) = 4kT(t/\pi C\rho)^{1/2} \quad (12.42)$$

and the bending decay function is

$$\Delta(t) = B(t)\, t^{1/4} \quad (12.43)$$

In these equations k is Boltzmann's constant, T is the temperature, C is the torsional stiffness of DNA, and ρ is a frictional coefficient per unit length for rotation about the helix axis. $B(t)$ is a slowly varying function of time that is determined by the bending stiffness of DNA. Eqs. 12.41–12.43 shows that the anisotropy decay depends on $t^{1/2}$ due to torsional or twisting motions, and $t^{1/4}$ due to bending motions.

For ns decay times the bending motions have little effect on the anisotropy decay. Hence, one often encounters these equations in a more simplified form:[74]

$$r(t) = r_0[0.75 \exp(-t/\theta_1)^{1/2} + 0.25] \quad (12.44)$$

where

$$\theta_1 = \pi^2 b^2 \eta C/4k^2T^2 \quad (12.45)$$

where b is the radius of DNA and η is viscosity.

Most of the anisotropy decays of EB bound to DNA are visually similar (Figure 12.31).[74–78] The anisotropy decays rapidly at early times, and tends towards a constant value at longer times. The early portion of the anisotropy decay is due to the torsional motions of DNA. The constant anisotropy at longer times is due to the bending motions, which are not significant on this timescale.

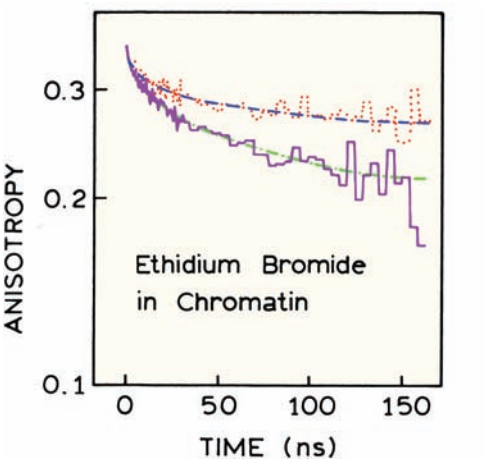

Figure 12.31. Fluorescence anisotropy decay curves of intercalated ethidium in chromatin DNA. Buffer conditions were 1 mM Tris and 0.2 mM EDTA, pH 7.5 (solid), and 50 mM NaCl, 1 mM Tris, and 0.2 mM EDTA, pH 7.5 (dotted). The temperature was 20°C. Revised and reprinted with permission from [78]. Copyright © 1983, American Chemical Society.

12.9. TRANSITION MOMENTS

Throughout this chapter we described the dependence of anisotropy on the direction of the transition moments. The existence of a discrete direction often seems somewhat mysterious because the experiments in isotropic solution do not reveal this direction in the molecule. The direction of transition moment can be determined if the fluorophores can be oriented. Molecules can be oriented in crystals, liquid crystals, oriented membranes, or stretched polymer films. Stretched films provide the easiest approach to obtaining oriented fluorophores, particularly if the molecules are elongated along one axis, and if uniaxial orientation is adequate.[79–82] The basic experiment is to dissolve the fluorophore and a polymer in a solvent. The polymer is typically polyvinyl alcohol. After removal of the solvent the polymer is then stretched about fivefold. For linear molecules like DPH and DAPI one can obtain nearly complete orientation along the stretching axis. Less asymmetric fluorophores are still aligned, but the orientation function can be more complex.[83]

An example of an oriented system is shown in Figure 12.32 for DPH in a stretched PVA film.[84] Prior to stretching

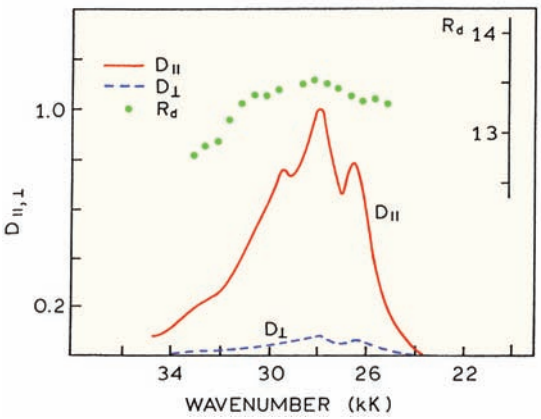

Figure 12.32. Absorption spectra of DPH parallel (||) and perpendicular (⊥) to the direction of stretching in a polyvinyl alcohol (PVA) film. $R_d = D_{||}/D_\perp$ is the dichroic ratio. Revised from [84].

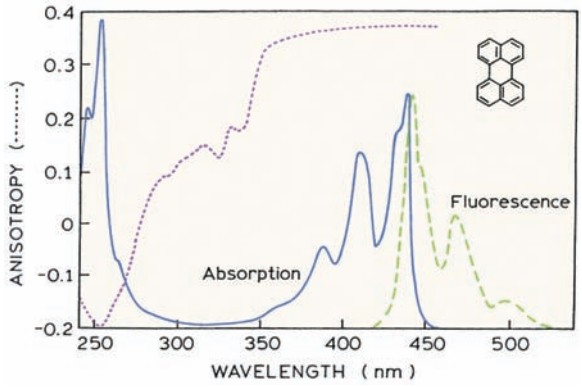

Figure 12.34. Absorption and excitation anisotropy spectra of perylene in propylene glycol.

the absorption spectra are independent of the orientation of the polarizer. After fivefold stretching, the sample absorbs strongly when the polarizer is oriented along the stretching axis, and the absorption is weak when the polarizer is perpendicular to this axis. Since the long axis of DPH orients parallel to the direction of stretching, these spectra provide an experimental demonstration that the transition moment of DPH is oriented along its long axis.

Recall from the theory of anisotropy (Section 10.2) that the highest anisotropy of 0.4 was a consequence of excitation photoselection, and that a single fluorophore oriented along the z-axis was predicted to have an anisotropy of 1.0. This prediction can be confirmed from experiments with stretched films (Figure 12.33). As the sample is stretched, the anisotropy of DPH increases well above 0.4, to about 0.82. The value is not 1.0 because the sample is not perfectly aligned, and the values of β for DPH obtained from $<\cos^2 \beta>$ seems to be about 8°. Such data have also been used to confirm the cosine-squared dependence of absorption.[85]

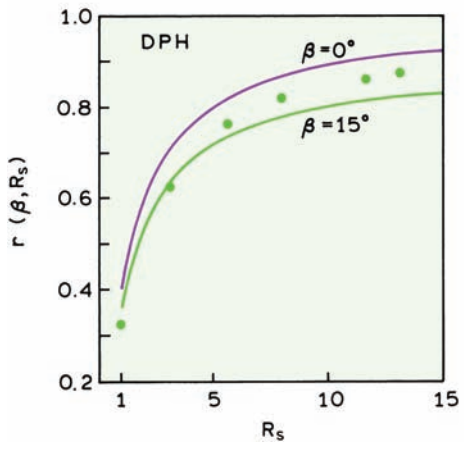

Figure 12.33. Steady-state anisotropy of DPH in polyvinyl alcohol (PVA). The lower axis shows the stretching ratio (R_s). The solid lines are theoretical curves for β = 0 and 15°. Revised from [84].

Perylene displays regions of high and low anisotropy (Figure 12.34). At wavelengths above 360 nm ($S_0 \rightarrow S_1$) the anisotropy is positive and nearly constant. At wavelengths below 280 nm ($S_0 \rightarrow S_2$) the anisotropy is negative. According to eq. 10.22 an anisotropy of –0.20 corresponds to an angle of 90° between the absorption and emission moments. This was demonstrated experimentally using the polarized absorption spectra of perylene (Figure 12.35).[83] The spectra are measured for light polarized parallel or perpendicular to the long axis of perylene. These spectra are calculated from the stretched film spectra. The long-wavelength absorption ($S_0 > S_1$) is thus seen to be oriented along the long axis, and the short-wavelength absorption is oriented along the short axis.

As a final example, Figure 12.36 shows the polarized absorption spectra of 9-aminoacridine, again recovered from the experimental spectra in PVA films.[86] In 9-aminoacridine the long-wavelength transition displays positive anisotropy, which one tends to associate with transitions along the long axis. However, the long-wavelength ($S_0 \rightarrow S_1$) transition is polarized along the short axis of the molecule. This result is counterintuitive because we generally assign the lowest energy transition to the longest axis. This result can be understood as the electronic charge moving between the two nitrogen atoms, each with a different elec-

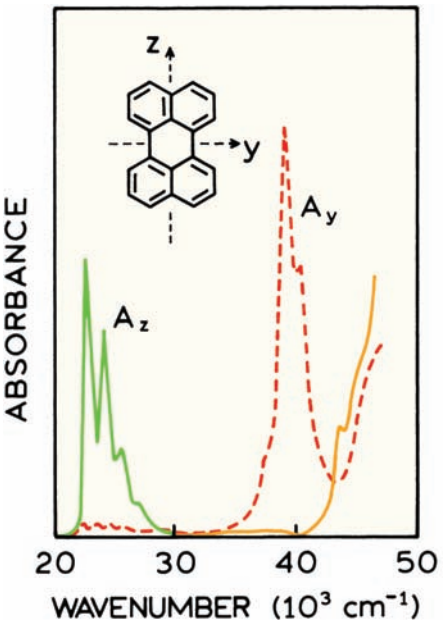

Figure 12.35. Absorption spectra of perylene along the long (z) and short (y) axes. Revised from [83].

tron density. Absorption spectra in stretched films have been used to determine the direction of transition moments in a number of fluorophores of biochemical interest, including adenine,[87] 2-aminopurine,[88] Yt-base[89], DAPI,[90] Hoechst 33342,[85] and polynuclease aromatic hydrocarbons.[91]

12.9.1. Anisotropy of Planar Fluorophores with High Symmetry

The fundamental anisotropy can be determined in part by the symmetry of the molecule. This is illustrated by triphenylene, which has threefold symmetry and a fundamental

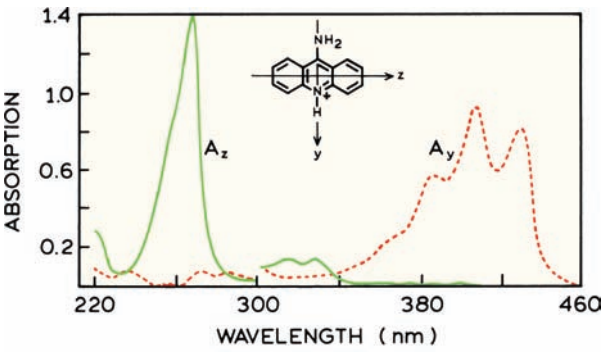

Figure 12.36. Polarized absorption spectra of 9-aminoacridinium in a stretched PVA film. Revised from [86].

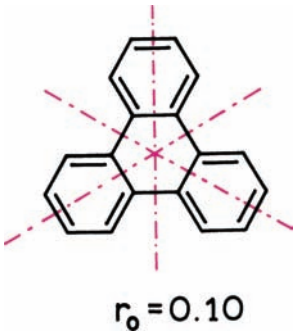

Figure 12.37. Structure and symmetry axes of triphenylene.

anisotropy of r_0 = 0.1 (Figure 10.37).[92] This anisotropy value is found whenever the transition moments are randomized in a plane. The anisotropy value of 0.1 can be calculated from the additivity law of anisotropy (eq. 10.6). Following excitation along one of the axes the emission is randomized among the three identical axes. Since the axes are identical, a third of the emission originates from each transition, resulting in r_0 = 0.10 (Problem 12.3).

12.10. LIFETIME-RESOLVED ANISOTROPIES

In Sections 10.5 and 10.6 we saw how the Perrin equation could be used to estimate the apparent volume of macromolecule. Examination of eq. 10.45 suggests an alternative method of estimating the rotational correlation time. Suppose the lifetime (τ) of the probe could be decreased by collisional quenching. Then a plot of $1/r$ versus τ would have a slope of $(r_0/\theta)^{-1}$, and thus allow measurement of the correlation time. These measurements are called lifetime-resolved anisotropies.[93–98] The first suggestion of lifetime-resolved anisotropies appeared early in the literature as a means to study polymers[98–99] as well as proteins.[100]

There are advantages to the use of lifetime-resolved measurements. The lifetime can typically be decreased with only a modest change in solution conditions. This is particularly true for oxygen quenching since oxygen diffuses rapidly and is an efficient quencher. The use of oxygen quenching is demonstrated in Figure 12.38, which shows anisotropy values of a peptide hormone when the single-tryptophan residue was quenched to various lifetimes.[101] The proteins were human luteinizing hormone (hLH) and its β subunit (βhLH). The intact hormone has a molecular weight of 28 kD, and the β subunit is 14 kD. The apparent correlation times were 6.0 and 4.9 ns, respectively. The calculated correlation times are 10.1 and 5.2 ns, respectively. The meas-

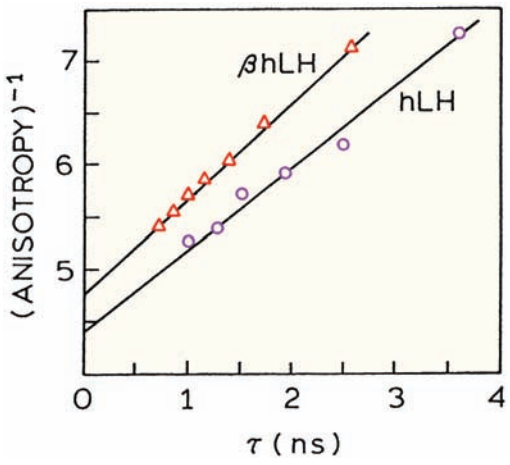

Figure 12.38. Lifetime-resolved anisotropies of human luteinizing hormone (hLH) and its β subunit. The lifetimes were varied by oxygen quenching, and calculated from the dynamic portion of the observed quenching. Revised and reprinted with permission from [101]. Copyright © 1987, American Chemical Society.

ured and calculated values are reasonably close, but the *y*-intercepts yield apparent r_0 values smaller than the expected value of 0.27. This result is typical of other reports that suggest segmental freedom of tryptophan residue in many proteins.[93–96]

12.10.1. Effect of Segmental Motion on the Perrin Plots

The effect of segmental motion on the Perrin plots can be seen by deriving the Perrin equation for the anisotropy decay expected in the presence of segmental motions. While the results are the same whether one measures anisotropy versus T/η, or versus lifetime, these effects are somewhat easier to understand in terms of the lifetime-resolved measurements. In addition, the experiments are easier to interpret because the temperature and solution conditions are not changed, so that changes in protein dynamics and conformation do not complicate the analysis.

Suppose a fraction α of the total anisotropy is lost by the segmental motion, with a fast correlation time θ_F, and the remainder of the anisotropy decays by overall rotational diffusion of the protein (θ_P). For independent segmental motions and rotational diffusion the anisotropy is given as the product of the depolarization factors, so that

$$r(t) = r_0\left[\alpha \exp(-t/\theta_F) + (1-\alpha)\right]\exp(-t/\theta_P) \qquad (12.46)$$

where $f_F + f_P = 1.0$. Use of eq. 10.43 with eq. 12.46 yields

$$r(\tau) = \frac{\alpha r_0}{1 + \left(\frac{1}{\theta_F} + \frac{1}{\theta_P}\right)\tau} + \frac{(1-\alpha)r_0}{1 + \frac{\tau}{\theta_P}} \qquad (12.47)$$

In this expression we used the notation $r(\tau)$ as a reminder that the steady-state anisotropy depends on the lifetime τ. In many cases the internal motions are more rapid than overall rotation ($\theta_F << \theta_P$), simplifying eq. 12.47 to

$$r(\tau) = \frac{\alpha r_0}{1 + \tau/\theta_F} + \frac{r_0(1-\alpha)}{1 + \tau/\theta_P} \qquad (12.48)$$

This expression indicates that a fraction of the anisotropy (αr_0) is lost due to the rapid motion, and the remainder $r_0(1-\alpha)$ is lost due to overall rotational diffusion.

The effects of varying degrees of segmental motion are shown in Figure 12.39. The assumed correlation times were $\theta_P = 20$ ns for overall rotational diffusion and $\theta_F = 1.0$ or 0.1 ns for the rapid motion. As the amplitude of the fast motion increases the *y*-intercept increases. This shows how segmental motions in proteins result in low apparent r_0 values. Perhaps more important is the observation that the apparent correlation times (θ_A), calculated from the limiting slope of the lifetime Perrin plots, decrease as α increases. This illustrates how segmental freedom in a protein can result in apparent correlation times that are lower than the true values. These simulated data are for lifetime-resolved measurements, but similar effects can be seen in simulated T/η Perrin plots.

12.11. SOLEILLET'S RULE: MULTIPLICATION OF DEPOLARIZATION FACTORS

In Chapter 10 we derived the value of r_0 expected due to photoselection ($r_0 = 0.4$), showed how r_0 was decreased by a factor dependent on the angle β between the absorption and emission transition moments (eq. 10.22), and that the anisotropy was decreased further due to rotational diffusion (eq. 10.44). There is a simple relationship between these different causes of depolarization, which is known as Soleillet's rule.[102–104] The anisotropy is given by the product of the various depolarization factors that occur in a given sample:

$$r = r_0 \prod_i d_i \qquad (12.49)$$

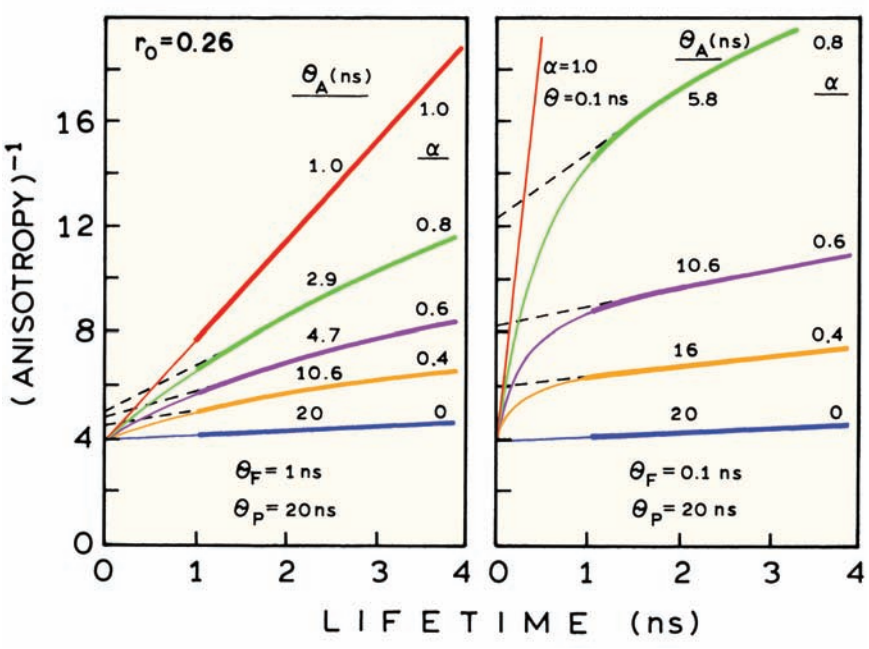

Figure 12.39. Simulated lifetime Perrin plots for a protein with an overall correlation time θ_P = 20 ns, and a fast segmental motion with θ_F = 1.0 or 0.1 ns. Revised and reprinted with permission from [94]. Copyright © 1983, American Chemical Society.

where d_i represents the extent to which anisotropy is decreased by each depolarization factor. This relationship can be clarified by a specific example. Suppose a fluorophore has an anisotropy less than 0.4 due to a displacement of the transition moment by an angle β and due to rotational diffusion. The steady-state anisotropy can be written as

$$r = d_1 d_2 d_3 = \frac{2}{5}\left(\frac{3\langle\cos^2\beta\rangle - 1}{2}\right)\left(\frac{3\langle\cos^2\omega\rangle - 1}{2}\right) \quad (12.50)$$

In this expression the first depolarization factor (d_1) is 0.4, which accounts for excitation photoselection $\langle\cos^2\theta\rangle$ (eq. 10.20). The second term (d_2) accounts for the angle between the transition moments $\langle\cos^2\beta\rangle$ (eq. 10.22). The third term (d_3) is the average angular (ω) displacement of the fluorophore during the excited state lifetime $\langle\cos^2\omega\rangle$. This factor is also given by $d_3 = (1 + \tau/\theta)^{-1}$ (eq. 10.44). It is sometimes useful to be aware of Soleillet's rule when attempting to account for the overall loss of anisotropy.

12.12. ANISOTROPIES CAN DEPEND ON EMISSION WAVELENGTH

The anisotropy is generally independent of the emission wavelength. However, the presence of time-dependent spectral relaxation (Chapter 7) can result in a substantial decrease in anisotropy across the emission spectrum.[105–108] A biochemical example is shown in Figure 12.40 for egg PC vesicles labeled with 12-AS. Because of time-dependent reorientation of the local environment around the excited state of 12-AS, the emission spectra display a time-dependent shift to longer wavelengths.[109] Such relaxation is often analyzed in terms of the time-resolved emission spectra, but one can also determine the mean lifetime at various emission wavelengths (Figure 12.40, bottom). The mean lifetime increases with wavelength because the lifetime at short wavelengths is decreased by relaxation, and long-wavelength observation selects for the relaxed species.

Recall that the steady-state anisotropy is determined by $r(t)$ averaged over $I(t)$ (eq. 10.43), resulting in Perrin eq. 10.44. Because of the longer average lifetime at long wavelengths, the anisotropy decreases with increasing wave-

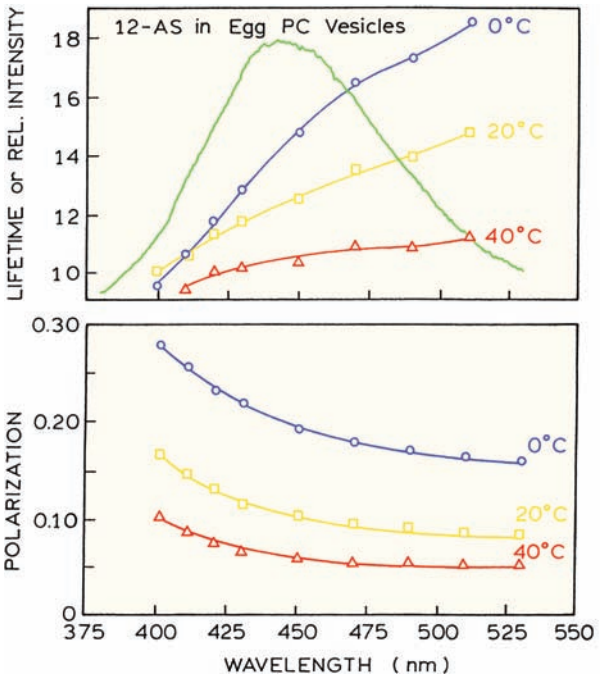

Figure 12.40. Average lifetime of 12-AS in egg PC vesicles (top) and the emission anisotropy (bottom). The average lifetimes were determined from the phase shift at 30 MHz. Revised from [109].

length (Figure 12.40). If the fluorophores were in a very fluid or glassy solvent, the lifetime and anisotropy would be constant across the emission spectrum.

REFERENCES

1. Bialik CN, Wolf B, Rachofsky EL, Ross JBA, Laws WR. 1998. Dynamics of biomolecules: assignment of local motions by fluorescence anisotropy decay. *Biophys J* **75**:2564–2573.
2. Vyleta NP, Coley AL, Laws WR. 2004. Resolution of molecular dynamics by time-resolved fluorescence anisotropy: verification of two kinetic models. *J Phys Chem A* **108**:5156–5160
3. Rachofsky EL, Laws WR. 2000. Kinetic models and data analysis methods for fluorescence anisotropy decay. *Methods Enzymol* **321**:216–238.
4. Brand L, Knutson JR, Davenport L, Beechem JM, Dale RE, Walbridge DG, Kowalczyk AA. 1985. Time-resolved fluorescence spectroscopy: Some applications of associative behaviour to studies of proteins and membranes. In *Spectroscopy and the dynamics of molecular biological systems*, pp. 259–305. Ed P Bayley, RE Dale. Academic Press London.
5. Fisz JJ. 1996. Polarized fluorescence decay surface for a mixture of non-interacting species in solution. *Chem Phys Lett* 259:579–587.
6. Fisz JJ. 1996. Polarized fluorescence spectroscopy of two-ground and two-excited state systems in solutions. *Chem Phys Lett* **262**: 495–506.
7. Fisz JJ. 1996. Polarized fluorescence decay surface for many-ground- and many-excited-state species in solution. *Chem Phys Lett* **262**:507–518.
8. Bialik CN, Wolf B, Rachofsky EL, Ross JBA, Laws WR. 1998. Fluorescence anisotropy decay: finding the correct physical model. *SPIE Proc* **3526**:60–67.
9. Wolber PK, Hudson BS. 1981. Fluorescence lifetime and time-resolved polarization anisotropy studies of acyl chain order and dynamics in lipid bilayers. *Biochemistry* **20**:2800–2816.
10. Wolber PK, Hudson BS. 1982. Bilayer acyl chain dynamics and lipid–protein interaction. *Biophys J* **37**:253–262.
11. Ruggiero A, Hudson B. 1989. Analysis of the anisotropy decay of trans-parinaric acid in lipid bilayers. *Biophys J* **55**:1125–1135.
12. van Paridon PA, Shute JK, Wirtz KWA, Visser AJWG. 1988. A fluorescence decay study of parinaroyl-phosphatidylinositol incorporated into artificial and natural membranes. *Eur Biophys J* **16**:53–63.
13. Visser AJWG, van Hoek A, van Paridon PA. 1987. Time-resolved fluorescence depolarization studies of parinaroyl phosphatidylcholine in triton X-100 micelles and rat skeletal muscle membranes. In *Membrane receptors, dynamics, and energetics*, pp. 353–361. Ed KWA Wirtz. Plenum Publishing, New York.
14. Millar DP, Allen DJ, Benkovic SJ. 1990. Structure and dynamics of a DNA: polymerase complex by time-resolved fluorescence spectroscopy. *SPIE Proc* **1204**:392–403.
15. Guest CR, Hochstrasser RA, Dupuy CG, Allen DJ, Benkovic SJ, Millar DM. 1991. Interaction of DNA with the Klenow fragment of DNA polymerase I studied by time-resolved fluorescence spectroscopy. *Biochemistry* **30**:8759–8770.
16. Peng K, Visser AJWG, van Hoek A, Wolfs CJAM, Sanders JC, Hemminga MA. 1990. Analysis of time-resolved fluorescence anisotropy in lipid–protein systems, I: application to the lipid probe octadecyl rhodamine B in interaction with bacteriophage M13 coat protein incorporated in phospholipid bilayers. *Eur Biophys J* **18**: 277–283.
17. Peng K, Visser AJWG, van Hoek A, Wolfs CJAM, Hemminga MA. 1990. Analysis of time-resolved fluorescence anisotropy in lipid–protein systems, II: application to tryptophan fluorescence of bacteriophage M13 coat protein incorporated in phospholipid bilayers. *Eur Biophys J* **18**:285–293.
18. Smith TA, Irwanto M, Haines DJ, Ghiggino KP, Millar DP. 1998. Time-resolved fluorescence anisotropy measurements of the adsorption of Rhodamine-B and a labelled polyelectrolyte onto colloidal silica. *Colloid Polym Sci* **276**:1032–1037.
19. Bailey MF, Thompson EHZ, Millar DP. 2001. Probing DNA polymerase fidelity mechanisms using time-resolved fluorescence anisotropy. *Methods* **25**:62–77.
20. Szmacinski H, Jayaweera R, Cherek H, Lakowicz JR. 1987. Demonstration of an associated anisotropy decay by frequency-domain fluorometry. *Biophys Chem* **27**:233–241.
21. Wang R, Bright FV. 1993. Rotational reorientation kinetics of dansylated bovine serum albumin. *J Phys Chem* **97**:4231–4238.
22. Perrin F. 1929. Mouvement brownien d'un ellipsoide (I): dispersion dielectrique pour ds molecules ellipsoidales. *J Phys Radium* **7**(5): 497–511.
23. Perrin F. 1936. Mouvement brownien d'un ellipsoide (II): rotation libre et depolarisation des fluorescences. Translation et diffusin de molecules ellipsoidales. *J Phys Radium* **7**(7):1–11.

24. Perrin F. 1936. Diminution de la polarisation de (I): fluorescence des solutions resultant du mouvement brownien de rotation. *Acta Phys Pol* **5**:335–345.
25. Perrin F. 1929. La fluorescence des solutions: induction moleculaire-polarisatron et duree d'emission-photochemie. *Ann Phys* **12**:169–275.
26. Lombardi JR, Dafforn GA. 1966. Anisotropic rotational relaxation in rigid media by polarized photoselection. *J Chem Phys* **44**:3882–3887.
27. Tao T. 1969. Time-dependent fluorescence depolarization and Brownian rotational diffusion of macromolecules. *Biopolymers* **8**: 609–632.
28. Ehrenberg M, Rigler R. 1972. Polarized fluorescence and rotational Brownian rotation. *Chem Phys Lett* **14**:539–544.
29. Chuang TJ, Eisenthal KB. 1972. Theory of fluorescence depolarization by anisotropic rotational diffusion. *J Chem Phys* **57**:5094–5097.
30. Belford GG, Belford RL, Weber G. 1972. Dynamics of fluorescence polarization in macromolecules. *Proc Natl Acad Sci USA* **69**:1392–1393.
31. Small EW, Isenberg I. 1977. Hydrodynamic properties of a rigid molecule: rotational and linear diffusion and fluorescence anisotropy. *Biopolymers* **16**:1907–1928.
32. Weber G. 1989. Perrin revisited: parametric theory of the motional depolarization of fluorescence. *J Phys Chem* **93**:6069–6073.
33. Piston DW, Bilash T, Gratton E. 1989. Compartmental analysis approach to fluorescence anisotropy: perylene in viscous solvents. *J Phys Chem* **93**:3963–3967.
34. Irving M. 1996. Steady-state polarization from cylindrically symmetric fluorophores undergoing rapid restricted motion. *Biophys J* **70**:1830–1835.
35. Feinstein E, Deikus G, Rusinova E, Rachofsky EL, Ross JBA, Laws WR. 2003. Constrained analysis of fluorescence anisotropy decay: application to experimental protein dynamics. *Biophys J* **84**:599–611.
36. Steiner RF. 1991. Fluorescence anisotropy: theory and applications. In *Topics in fluorescence spectroscopy*, Vol. 2: *Principles*, pp. 1–52. Ed JR Lakowicz. Plenum Press, New York.
37. Barkley MD, Kowalczyk AA, Brand L. 1981. Fluorescence decay studies of anisotropic rotations: Internal motions in DNA. In *Biomolecular stereodynamics*, Vol. 1, pp. 391–403. Ed RH Sarma. Adenine Press, New York.
38. Beechem JM, Knutson JR, Brand L. 1986. Global analysis of multiple dye fluorescence anisotropy experiments on proteins. *Biochem Soc Trans* **14**:832–835.
39. Kawski A. 1993. Fluorescence anisotropy: theory and applications of rotational depolarization. *Crit Rev Anal Chem* 23(6):459–529.
40. Tan X, Gustafson TL. 2000. Solvent–solute interactions probed by picosecond time-resolved fluorescence spectroscopy: lifetime and anisotropy study of S_1 *trans*-4,4'-diphenylstilbene. *J Phys Chem A* 104:4469–4474.
41. Dutt GB, Ghanty TK. 2003. Rotational dynamics of nondipolar probes in ethanols: how does the strength of the solute–solvent hydrogen bond impede molecular rotation? *J Chem Phys* **119**(9): 4768–4774.
42. Ito N, Kajimoto O, Hara K. 2002. High-pressure studies of rotational dynamics for coumarin 153 in alcohols and alkanes. *J Phys Chem A* **106**:6024–6029.
43. Singh MK. 2000. Rotational relaxation of neutral red in alkanes: effect of solvent size on probe rotation. *Photochem Photobiol* **72**(4):438–443.
44. Jas GS, Larson EJ, Johnson CK, Kuczera K. 2000. Microscopic details of rotational diffusion of perylene in organic solvents: molecular dynamics simulation and experiment vs Debye-Stokes-Einstein theory. *J Phys Chem A* **104**:9841–9852.
45. Brocklehurst B, Young RN. 1999. Rotation of aromatic hydrocarbons in viscous alkanes, 1: methylcyclohexane. *J Phys Chem A* **103**: 3809–3817.
46. Dutt GB. 2000. Rotational dynamics of nondipolar probes in alkane–alkanol mixtures: microscopic friction on hydrogen bonding and nonhydrogen bonding solute molecules. *J Chem Phys* **113**(24): 11154–11158.
47. Hu C-M, Zwanzig R. 1974. Rotational friction coefficients for spheroids with the slipping boundary condition. *J Chem Phys* **60**(11): 4354–4357.
48. Youngren GK, Acrivos A. 1975. Rotational friction coefficients for ellipsoids and chemical molecules with the slip boundary condition. *J Chem Phys* **63**:3846–3848.
49. Barkley MD, Kowalczyk AA, Brand L. 1981. Fluorescence decay studies of anisotropic rotations of small molecules. *J Chem Phys* **75**(7):3581–3593.
50. Brocklehurst B, Young RN. 1994. Fluorescence anisotropy decays and viscous behaviour of 2-methyltetrahydrofuran. *J Chem Soc Faraday Trans* **90**(2):271–278.
51. Brocklehurst B, Young RN. 1995. Rotation of perylene in alkanes: nonhydrodynamic behavior. *J Phys Chem* **99**:40–53.
52. Sasaki T, Hirota K, Yamamoto M, Nishijima K. 1987. Anisotropic rotation of perylene studied by fluorescence depolarization method. *Bull Chem Soc Jpn* **60**:1165–1167.
53. Viovy JL. 1985. Anisotropic rotation of 1,9-dimethylanthracene: a fluorescence anisotropy decay study. *J Phys Chem* **89**:5465–5472.
54. Weber G. 1977. Theory of differential phase fluorometry: detection of anisotropic molecular rotations. *J Chem Phys* **66**(9):4081–4091.
55. Mantulin WW, Weber G. 1977. Rotational anisotropy and solvent-fluorophore bond: an investigation by differential polarized phase fluorometry. *J Chem Phys* **66**(9):4092–4099.
56. Weber G, Mitchell GW. 1976. Demonstration of anisotropic molecular rotations by differential polarized phase fluorometry. In *Excited states of biological molecules*, pp. 72–76. Ed JB Birks. John Wiley & Sons, New York.
57. Lakowicz JR, Prendergast FG, Hogen D. 1979. Differential polarized phase fluorometric investigations of diphenylhexatriene in lipid bilayers: quantitation of hindered depolarizaing rotations. *Biochemistry* **18**:508–519.
58. Klein UKA, Haas HP. 1979. Picosecond rotational diffusion of perylene. *Chem Phys Lett* **63**(1):40–42.
59. Lakowicz JR, Gryczynski I. 1991. Frequency-domain fluorescence spectroscopy. In *Topics in fluorescence spectroscopy*, Vol. 1: *Techniques*, pp. 293–355. Plenum Press, New York.
60. Lakowicz JR, Cherek H, Maliwal BP. 1985. Time-resolved fluorescence anisotropies of diphenylhexatriene and perylene in solvents and lipid bilayers obtained from multifrequency phase-modulation fluorometry. *Biochemistry* **24**:376–383.

61. Lakowicz JR, Maliwal BP. 1985. Construction and performance of a variable-frequency phase-modulation fluorometer. *Biophys Chem* **21**:61–78.
62. Lakowicz JR, Gryczynski I, Cherek H, Laczko G. 1991. Anisotropy decays of indole, melittin monomer and melittin tetramer by frequency-domain fluorometry and multi-wavelength global analysis. *Biophys Chem* **39**:241–251.
63. Gryczynski I, Cherek H, Laczko G, Lakowicz JR. 1987. Enhanced resolution of anisotropic rotational diffusion by multi-wavelength frequency-domain fluorometry and global analysis. *Chem Phys Lett* **135**(3):193–199.
64. Gryczynski I, Cherek H, Lakowicz JR. 1988. Detection of three rotational correlation times for a rigid asymmetric molecule using frequency-domain fluorometry. *SPIE Proc* **909**:285–292.
65. Gryczynski I, Danielson E, Lakowicz JR. Unpublished observations.
66. Lakowicz JR, Gryczynski I, Wiczk WM. 1988. Anisotropic rotational diffusion of indole in cyclohexane studied by 2 GHz frequency-domain fluorometry. *Chem Phys Lett* **149**(2):134–139.
67. Gryczynski I, Cherek H, Lakowicz JR. 1988. Detection of three rotational correlation times for a rigid asymmetric molecule using frequency-domain fluorometry. *Biophys Chem* **30**:271–277.
68. Gryczynski I, Wiczk W, Johnson ML, Lakowicz JR. 1988. Lifetime distributions and anisotropy decays of indole fluorescence in cyclohexane/ethanol mixtures by frequency-domain fluorometry. *Biophys Chem* **32**:173–185.
69. Lakowicz JR, Cherek H, Gryczynski I, Joshi N, Johnson ML. 1987. Enhanced resolution of fluorescence anisotropy decays by simultaneous analysis of progressively quenched samples. *Biophys J* **51**: 755–768.
70. Lakowicz JR, Gryczynski I, Szmacinski H, Cherek H, Joshi N. 1991. Anisotropy decays of single-tryptophan proteins measured by GHz frequency-domain fluorometry with collisional quenching. *Eur Biophys J* **19**:125–140.
71. Barkley MD, Zimm BH. 1979. Theory of twisting and bending of chain macromolecules; analysis of the fluorescence depolarization of DNA. *J Chem Phys* **70**(6):2991–3007.
72. Thomas JC, Allison SA, Appellof CJ, Schurr JM. 1980. Torsion dynamics and depolarization of fluorescence of linear macromolecules, II: fluorescence polarization anisotropy measurements on a clean viral 29 DNA. *Biophys Chem* **12**:177–188.
73. Schurr JM, Fujimoto BS, Wu P, Song L. 1992. Fluorescence studies of nucleic acids: dynamics, rigidities, and structures. In *Topics in fluorescence spectroscopy*, Vol. 3: *Biochemical applications*, pp. 137–229. Ed JR Lakowicz. Plenum Press, New York.
74. Millar DP, Robbins RJ, Zewail AH. 1981. Time-resolved spectroscopy of macromolecules: effect of helical structure on the torsional dynamics of DNA and RNA. *J Chem Phys* **74**(7):4200–4201.
75. Ashikawa I, Furuno T, Kinosita K, Ikegami A, Takahashi H, Akutsu H. 1983. Internal motion of DNA in bacteriophages. *J Biol Chem* **259** (13):8338–8344.
76. Ashikawa I, Kinosita K, Ikegami A. 1984. Dynamics of z-form DNA. *Biochim Biophys Acta* **782**:87–93.
77. Genest D, Wahl Ph, Erard M, Champagne M, Daune M. 1982. Fluorescence anisotropy decay of ethidium bromide bound to nucleosomal core particles. *Biochim.* **64**:419–427.
78. Ashikawa, I., Kinosita, K., Ikegami, A., Nishimura, Y., Tsuboi, M., Watanabe, K., Iso, K., and Nakano, T., 1983. Internal motion of deoxyribonucleic acid in chromatin. Nanosecond fluorescence studies of intercalated ethidium. *Biochemistry* **22**:6018–6026.
79. Thulstrup EW, Michl J. 1988. Polarized absorption spectroscopy of molecules aligned in stretched polymers. *Spectrochim Acta* **A44**:767–782.
80. Michl J, Thulstrup EW. 1987. Ultraviolet and infrared linear dichroism: polarized light as a probe of molecular and electronic structure. *Acc Chem Res* **20**:192–199.
81. Van Gurp M, Levine YK. 1989. Determination of transition moment directions in molecules of low symmetry using polarized fluorescence, I: theory. *J Chem Phys* **90**(8):4095–4100.
82. Matsuoka Y, Yamaoka K. 1980. Film dichrosim, V: linear dichroism study of acridine dyes in films with emphasis on the electronic transitions involved in the long-wavelength band of the absorption spectrum. *Bull Chem Soc Jpn* **53**:2146–2151.
83. Michl J, Thulstrup EW. 1986. *Spectroscopy with polarized light*. VCH Publishers, New York.
84. Kawski A, Gryczynski Z. 1986. On the determination of transition-moment directions from emission anisotropy measurements. *Z Naturforsch A* **41**:1195–1199.
85. Kawski A, Gryczynski Z, Gryczynski I, Lakowicz JR, Piszczek G. 1996. Photoselection of luminescent molecules in anisotropic media in the case of two-photon excitation, II: experimental studies of Hoechst 33342 in stretched poly(vinyl alcohol) films. *Z Naturforsch A* **51**:1037–1041.
86. Matsuoka Y, Norden B. 1982. Linear dichroism study of 9-substituted acridines in stretched poly(vinyl alcohol) film. *Chem Phys Lett* **85**(3):302–306.
87. Holmén A, Broo A, Albinsson B, Nordén B. 1997. Assignment of electronic transition moment directions of adenine from linear dichroism measurements. *J Am Chem Soc* **119**(50):12240–12250.
88. Holmén A, Nordén B, Albinsson B. 1997. Electronic transition moments of 2-aminopurine. *J Am Chem Soc* **119**(13):3114–3121.
89. Albinsson B, Kubista M, Sandros K, Nordén B. 1990. Electronic linear dichroism spectrum and transition moment directions of the hypermodified nucleic acid–base wye. *J Phys Chem* **94**:4006–4011.
90. Kubista M, Åkerman B, and Albinsson B. 1989. Characterization of the electronic structure of 4',6-diamidino-2-phenylindole. *J Am Chem Soc* **111**:7031–7035.
91. Andersen KB, Waluk J, Thulstrup EW. 1999. The electronic structure of carcinogenic dibenzopyrenes: linear dichroism, fluorescence polarization spectroscopy and quantum mechanical calculations. *Photochem Photobiol* **69**(2):158–166.
92. Hall RD, Valeur B, Weber G. 1985. Polarization of the fluorescence of triphenylene: a planar molecule with three-fold symmetry. *Chem Phys Lett* **116**(2,3):202–205.
93. Lakowicz JR, Weber G. 1980. Nanosecond segmental mobilities of tryptophan residues in proteins observed by lifetime-resolved fluorescence anisotropies. *Biophys J* **32**:591–601.
94. Lakowicz JR, Maliwal BP, Cherek H, Balter A. 1983. Rotational freedom of tryptophan residues in proteins and peptides. *Biochemistry* **22**:1741–1752.

95. Lakowicz JR, Maliwal BP. 1983. Oxygen quenching and fluorescence depolarization of tyrosine residues in proteins. *J Biol Chem* **258**(8):4794–4801.
96. Eftink M. 1983. Quenching-resolved emission anisotropy studies with single and multitryptophan-containing proteins. *Biophys J* **43**: 323–334.
97. Lakos Z, Szarka Á, Koszorús L, Somogyi B. 1995. Quenching-resolved emission anisotropy: a steady state fluorescence method to study protein dynamics. *J Photochem Photobiol B: Biol* **27**:55–60.
98. Bentz JP, Beyl P, Beinert G, Weill G. 1973. Simultaneous measurements of fluorescence polarization and quenching: a specially designed instrument and an application to the micro-browian motion of polymer chains. *Eur Polymer J* **11**:711–718.
99. Brown K, Soutar I. 1974. Fluorescence quenching and polarization studies of segmental motion in polystyrene. *Eur Polymer J* **10**: 433–437.
100. Chen RF. 1976. Quenching of the fluorescence of proteins by silver nitrate. *Arch Biochem Biophys* **168**:605–622.
101. Sanyal G, Charlesworth MC, Ryan RJ, Prendergast FG. 1987. Tryptophan fluorescence studies of subunit interaction and rotational dynamics of human luteinizing hormone. *Biochemistry* **26**: 1860–1866.
102. Soleillet P. 1929. Sur les paramètres charactérisant la polarisation partielle de la lumière dans les phénomènes de fluorescence. *Ann Phys Biol Med* **12**:23–97.
103. Kawski A. 1986. Fluorescence anisotropy as a source of information about different photophysical processes. In *Progress and trends in applied optical spectroscopy*, Vol. 13, pp. 6–34. Ed D Fassler, K-H Feller, B Wilhelmi. Teubner Verlagsgesellschaft, Leipzig.
104. Weber G. 1966. Polarization of the fluorescence of solutions. In *Fluorescence and phosphorescenc analysis*, pp. 217–240. Ed DM Hercules. John Wiley & Sons, New York.
105. Gurinovich GP, Sarzhevskii AM, Sevchenko AN. 1963. New data on the dependence of the degree of polarization on the wavelength of fluorescence. *Opt Spectrosc* **14**:428–432.
106. Mazurenko YT, Bakhshiev NG. 1970. Effect of orientation dipole relaxation on spectral, time, and polarization characteristics of the luminescence of solutions. *Opt Spectrosc* **28**:490–494.
107. Gakamskii DM, Nemkovich NA, Rubinov AN, Tomin VI. 1988. Light-induced rotation of dye molecules in solution. *Opt Specrosc* **64**(3):406–407.
108. Chattopadhyay A, Mukherjee S. 1999. Depth-dependent solvent relaxation in membranes: wavelength-selective fluorescence as a membrane dipstick. *Langmuir* **15**:2142–2148.
109. Matayoshi ED, Kleinfeld AM. 1981. Emission wavelength-dependent decay of the 9-anthroyloxy-fatty acid membrane probes. *Biophys J* **35**:215–235.

PROBLEMS

P12.1. *Calculation of An Associated Anisotropy Decay*: Use the intensity and anisotropy decay in Figure 12.3 to calculate the anisotropy at t = 0, 1, and 5 ns. Also calculate the anisotropy values of 0, 1 and 5 ns assuming a non-associated anisotropy decay. What feature of the calculated values indicates the presence of an associated anisotropy decay?

P12.2. Figure 12.5 shows associated anisotropy decays for rhodamine B in water and bound to colloidal silica particles. Using the same parameter values, what is the form of the anisotropy decay for a non-associated model for the highest silica concentration? Describe the shape of the non-associated anisotropy decay.

P12.3. *Anisotropy of a Planar Oscillator*: Calculate the anisotropy of triphenylene assuming the emission is randomized among three equivalent axes (Figure 12.37).

P12.4. *Correlation Times from Lifetime-Resolved Anisotropies*: Figure 12.41 shows lifetime-resolved anisotropies of melittin. The lifetimes were varied by oxygen quenching. Calculate the correlation times and $r(0)$ values in 0 and 2.4 M NaCl, where melittin exists as a monomer and tetramer, respectively. Assume that the r_0 value for melittin is 0.26 and the monomeric molcular weight is 3250 daltons.

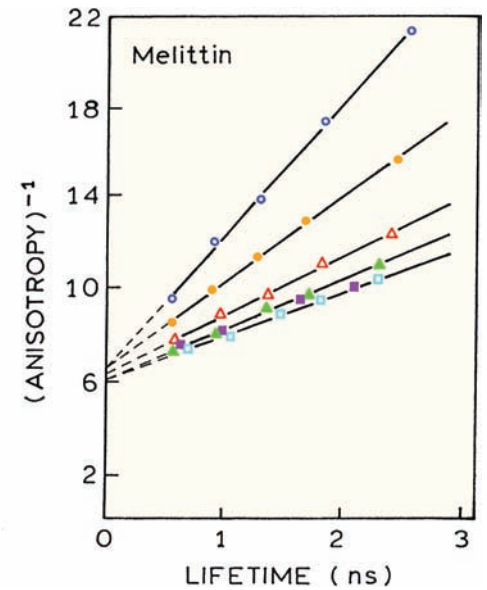

Figure 12.41. Lifetime-resolved anisotropy of melittin in aqueous buffer at 25°C. The concentrations of NaCl are 0 (open circles), 0.15 (solid circles), 0.3 (open triangles), 0.6 (solid triangles), 1.5 (solid squares), and 2.4 M (open squares). Revised and reprinted with permission from [94]. Copyright © 1983, American Chemical Society.